NASA CONTRACTOR
REPORT

NASA CR-2632

NASA CR-2632

THEORETICAL STUDY
OF REFRACTION EFFECTS
ON NOISE PRODUCED
BY TURBULENT JETS

E. W. Graham and B. B. Graham

Prepared by
GRAHAM ASSOCIATES
Shaw Island, Wash. 98286
for Langley Research Center

NATIONAL AERONAUTICS AND SPACE ADMINISTRATION • WASHINGTON, D. C. • DECEMBER 1975

1. Report No. NASA CR-2632	2. Government Accession No.	3. Recipient's Catalog No.
4. Title and Subtitle Theoretical Study of Refraction Effects on Noise Produced by Turbulent Jets		5. Report Date December 1975
		6. Performing Organization Code
7. Author(s) E. W. Graham and B. B. Graham		8. Performing Organization Report No.
		10. Work Unit No.
9. Performing Organization Name and Address Graham Associates Shaw Island, WA 98286		11. Contract or Grant No. NAS 1-12834
		13. Type of Report and Period Covered Contractor Report
12. Sponsoring Agency Name and Address National Aeronautics & Space Administration Washington, DC 20546		14. Sponsoring Agency Code
15. Supplementary Notes Technical monitors: Thomas D. Norum and Lucio Maestrello Final Report		

16. Abstract

The transmission of acoustic disturbances from the interior of a jet into the ambient air is studied here. The jet is assumed infintely long with mean velocity profile independent of stream-wise location. The noise generator is a sequence of transient sources drifting with the local fluid and confined to a short length of the jet.

In Part 1, supersonic jets are considered. Numerical results for mean-square pressure versus angle in the far-field show unexpected peaks which are very sharp. Analysis of simplified models indicates that these are complex quasi-resonant effects which appear to the stationary observer in a high frequency range. The peaks are real for the idealized model, but would be smoothed by mathematical integration over source position, velocity, and frequency. (Such smoothing is automatically achieved in experimental observations.) The computational difficulties produced by extremely high and narrow peaks may perhaps be avoided temporarily by excluding high observed frequencies.

In Part 2, subsonic jets are considered, and a preliminary study of the near-field is attempted. Mean-square radial displacements (or mean radial energy flow or space-time correlations of radial pressure gradient) are first found for very simple cases. The most difficult case studied is a sequence of transient sources at the center of a uniform-velocity circular cylindrical jet. Here a numerical triple integration is required and seems feasible although only preliminary results for mean-square radial displacement are now available.

These preliminary results show disturbances decreasing with increasing radial distance, and with increasing distance upstream and downstream from the source. A trend towards greater downstream disturbances appears even in the near-field.

17. Key Words (Suggested by Author(s)) Jet noise; refraction; convected wave equation; turbulence		18. Distribution Statement Unclassified - Unlimited Subject category 71	
19. Security Classif. (of this report) Unclassified	20. Security Classif. (of this page) Unclassified	21. No. of Pages 91	22. Price* $4.75

Table of Contents

NOMENCLATURE*

A   Source strength coefficient

c   Speed of sound

E   Energy flow per unit area

$\bar{E}$ Mean energy flow per unit area

i $\sqrt{-1}$

k_1 Wave number in x-direction (Cartesian coordinates)

k_2 Wave number in y-direction (Cartesian coordinates)

k   Wave number $= \sqrt{k_1^2 + k_2^2}$ (Cartesian coordinates);

Wave number in axial direction (cylindrical coordinates)

K_1 Reduced wave number in x-direction $= k_1/\omega'$ (Cartesian coordinates)

K_2 Reduced wave number in y-direction $= k_2/\omega'$ (Cartesian coordinates)

K   Reduced wave number $= k/\omega' = \sqrt{K_1^2 + K_2^2}$ (Cartesian coordinates);

Reduced wave number in axial direction $= k/\omega'$ (cylindrical coordinates)

M   Mach number

n   an integer

Δp Pressure increment from acoustic waves

$\overline{\Delta p^2}$ Mean-square pressure from acoustic waves

r   Radial cylindrical coordinate

----

*The secondary symbols not defined in this list are defined
where they are introduced in the analysis.

r_0	Radius of uniform velocity jet core
r_1	Radius of jet
r_s	Radial position of source
$\bar{r}_0$	r_0/r_1
$\bar{r}_s$	r_s/r_1
R	Radial spherical coordinate
S_T	Strouhal number
t	Time
x	Streamwise coordinate (coordinates fixed in source)
x_2	Streamwise coordinate (coordinates fixed in ambient air)
y	Lateral coordinate
z	Normal coordinate
R.P.	Denotes "real part of"
I.P.	Denotes "imaginary part of"
η	Radial displacement of a fluid particle
θ	Angular position in far field measured from upstream jet axis
ρ	Fluid density
ϕ	Velocity potential
ψ	Angle about x-axis (cylindrical coordinates)
ω	Generating frequency
ω'	ω/c
ω^*	Observed frequency
ω_0	Transient source frequency

Nomenclature, continued

Subscripts

c   refers to critical

j   refers to jet

s   refers to source

R   refers to real part

I   refers to imaginary part

THEORETICAL STUDY OF REFRACTION EFFECTS
ON NOISE PRODUCED BY TURBULENT JETS

E. W. Graham and B. B. Graham

Graham Associates, Shaw Island, Washington

INTRODUCTION

Objectives

This report is an extension of the work published in NASA CR-2390[1].
None of this work is intended as a comprehensive theory for the predic-
tion of noise produced by turbulence in jets. Instead we concentrate on
one aspect of this complex problem, the transmission of acoustical dis-
turbances from the interior of the jet into the ambient air. These
acoustical disturbances are generated by mathematically defined point
sources drifting with the local fluid. We neglect temporarily the more
difficult problem of identifying these mathematical sources with the
turbulence which they are intended to represent.

Because of the diversity of the material presented here (the far
field of supersonic jets as contrasted with the near field of subsonic
jets) this report is divided into two parts.

In Part 1 we study the peaks which arise in plots of mean-square
pressure versus angle in the far field for some supersonic jet examples.
Such peaks may occur even when the basic wavelength produced by the
pulsating source is several times the jet thickness. These peaks are so
severe in some instances that a pressure change of several orders of
magnitude may appear and disappear within a one degree change of angle
in the far field.

In Part 2 the near field disturbances created by transient sources
in a subsonic jet are studied. This is a preliminary attempt to get

theoretical data for comparison with the experimental in-house research work of NASA TN D-7269[2] by Maestrello. It may also be useful for checking the applicability of infinite-jet analysis to realistic expanding jets of finite length.

Related Work

This report and the preceding one, NASA CR-2390, utilize the radiation fields of sources convected with a moving fluid. Prior work of this type was done by Gottlieb[3], and by Moretti and Slutsky[4]. More recently an analysis of this type has been made by Mani[5].

Work on diverging jets (which are of course more realistically shaped than the cylindrical jets of the above literature) has been done by Schubert[6], by Liu and Maestrello[7], and by Padula and Liu[8]. We hope such analyses can be extended to cover sources convected with the moving fluid.

Possibly we have overlooked other closely related work which should be cited here, and certainly we have failed to refer to many jet noise studies which bear some relation to our own work. No disparagement of such omitted references is intended.

In our preceding report (NASA CR-2390) we should also have cited theoretical analyses by Mani[5] and by Morfey and Tanna[9], and experimental work by Ingard and Singhal[10], when mentioning the existence of more than one type of moving source.

Description of Model

The noise generator chosen is a sequence of transient sources drifting with the local fluid. The jet (either two-dimensional or circular cylindrical) extends to infinity upstream and downstream, with velocity profile independent of streamwise position. Thus the large velocity gradients across the jet are accounted for, and the smaller gradients in the streamwise direction are neglected. It seems reasonable to suppose that the major refraction effects will be shown by such a model. However investigation of the streamwise extent of near-field

2

disturbances may also cast light on the suitability of this model.

In making this analysis we consider that turbulence ("self-noise") is the only true originator of noise, and that "shear noise", being composed of linear terms, is part of the transmission process.

It must be emphasized that this is not a stability analysis. We deal with a distribution of turbulence in the jet which is essentially independent of time. This steady-state situation is the end result of the action of instabilities.

We then attempt to find the effect of the jet mean velocity profile on the transmission of acoustic disturbances from one element of turbulence through the jet and into the ambient air. The scattering effect of other elements of turbulence is neglected.

Description of Methods[*]

Generality of Methods[**]

Nearly all of the work in this report and the preceding report, NASA CR-2390, has in common certain necessary steps and concepts. The noise may be generated by sources (i.e. monopole sources), dipoles or quadrupoles. The noise generators may be on center, off center in a uniform velocity region or, in some cases, in the shear layer. Temperatures may be ambient or varying across the jet. The jet itself may be two-dimensional or circular. Still, with only minor modifications certain basic ideas apply, and we review them briefly.

For convenience we will describe the jet as being two-dimensional. The velocity profile must be independent of streamwise and lateral positions. For simplicity we will say "source", and speak of a single (constant velocity gradient) shear layer on each side of it, but other singularities can be used, and more complicated shear layers can be treated.

----

[*]Much of this is reproduced from NASA CR-2390 for the reader's convenience.

[**]See references 11-15.

The Source in a Jet

It is first assumed that the pulsating source is at rest in a completely stationary homogeneous fluid of infinite extent. The origin of coordinates is fixed in the source, and the conventional wave equation applies. The velocity potential produced by the source is readily expressed as the double integral of the velocity potentials for all reduced wave numbers, K_1 and K_2 in the s (streamwise) and y (lateral) directions. This corresponds to the decomposition of the source potential into an infinite set of plane waves (and exponential disturbances).

The source and some portion of the surrounding fluid at rest must next be confined within a jet. From coordinates fixed in the source this jet is seen as shear layers flowing past on each side, and outside the shear layers the ambient fluid flowing by at a fixed velocity. (See Fig. 1.) To accomplish this insertion of the source into the jet one must add to its original velocity potential the potentials for upward-moving and downward-moving waves reflected off the shear layers. These two reflected wave amplitudes are as yet unknown.

The Shear Layers and Ambient Air

In the shear layers the conventional wave equation does not apply. The correct partial differential equation is derived, and by assuming periodic solutions in the streamwise and lateral directions an ordinary differential equation is obtained in the coordinate normal to the shear layers. The ordinary differential equation is solved by power series expansions about the singular point, or about other points, and two independent solutions are obtained (in each layer) with amplitudes as yet unknown.

In the ambient air the conventional wave equation applies again (for coordinates fixed in the ambient fluid). Only outward moving waves need be considered, so (in each ambient region) one solution of unknown amplitude appears.

There are now eight unknown amplitudes to be determined and four boundaries between fluid layers. Across each of these boundaries pressure and displacement must be continuous, yielding the necessary eight
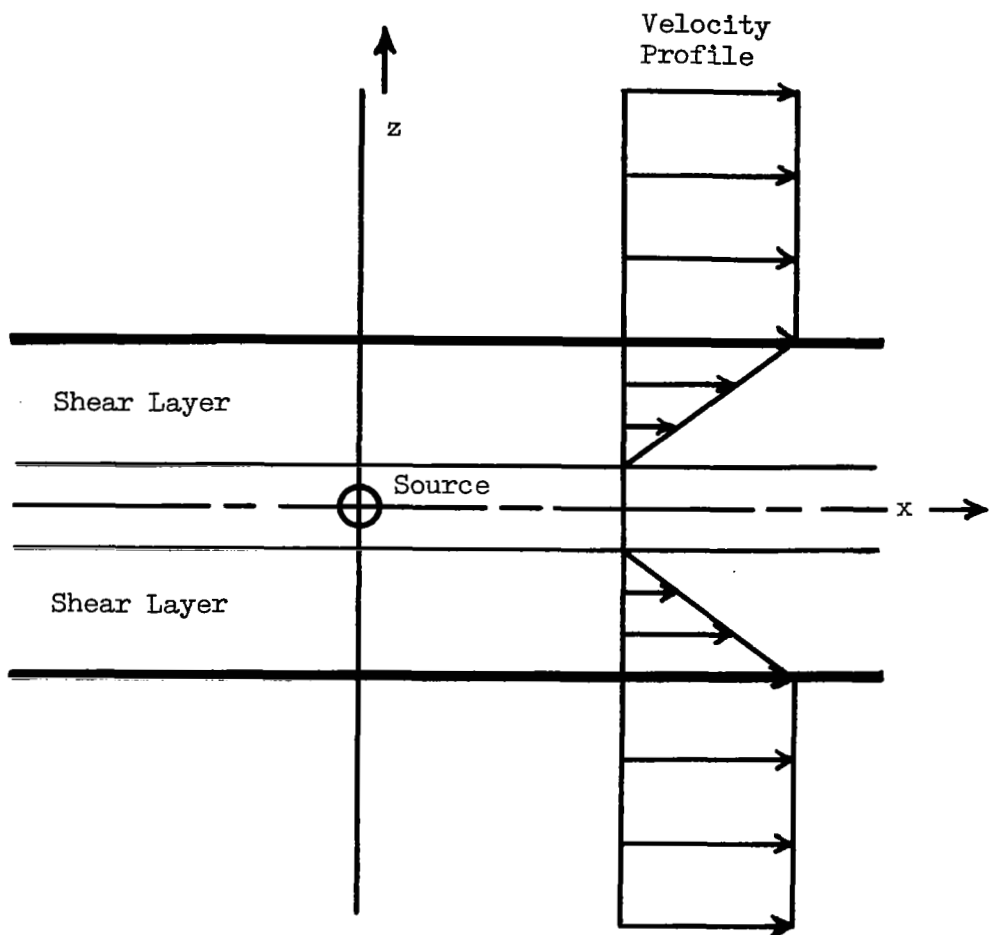
Fig. 1   COORDINATE SYSTEM FIXED IN SOURCE
          AND CORRESPONDING VELOCITY PROFILE

equations to make the system determinate. A double integral (over K_1 and K_2) for velocity potential in the ambient air is then obtained as a function of source strength and frequency.

The Far Field

Only in the far field can this double integral be evaluated easily. There the integrand generally consists of a slowly varying function multiplying a function which oscillates rapidly about zero. Such functions interact weakly, and significant contributions to the integral occur only when (a) the slowly varying function becomes rapidly varying (i.e. in the neighborhood of singular points) or (b) when the rapidly oscillating function ceases to be rapidly oscillating (i.e. in the neighborhood of stationary phase points). Evaluation of the integral yields the pressure in the far field for coordinates fixed in the source.

Transient Sources and Retarded Coordinates (the far field)

A more useful result would be the far-field mean-square pressure produced by sources in a localized region, say immediately behind a jet nozzle. To obtain this we consider a sequence of transient sources, each originating at the same point relative to the ambient air or nozzle. As one source disappears after drifting downstream with the fluid, a new one (with random phase relative to the first) appears at the upstream point. The mathematical analysis of this process (Ref. 13) is rather tedious. However the practical application conforms to a simple rule if it is assumed (as in the present analysis) that the transient sources have a lifetime of many cycles. The rule is that the mean-square pressure in source coordinates should first be formally transformed to retarded coordinates, fixed in the nozzle. (See Fig. 2.) The result must then be multiplied by $(1 + Mx_2/R)$, where M is the source Mach number relative to the ambient air, x_2 is the streamwise distance and R the radius to the far-field observation point.* (The rule holds also for the supersonic

----

*The factor $|1 + Mx_2/R|$ is often written $|1 + M\cos\theta|$ where θ is the angular position of the far-field observation point relative to the jet axis, $\theta = 0$ being measured upstream, $\theta = \pi$ downstream. The travel distance of each transient source and the thickness of the jet are of course negligible compared to R.
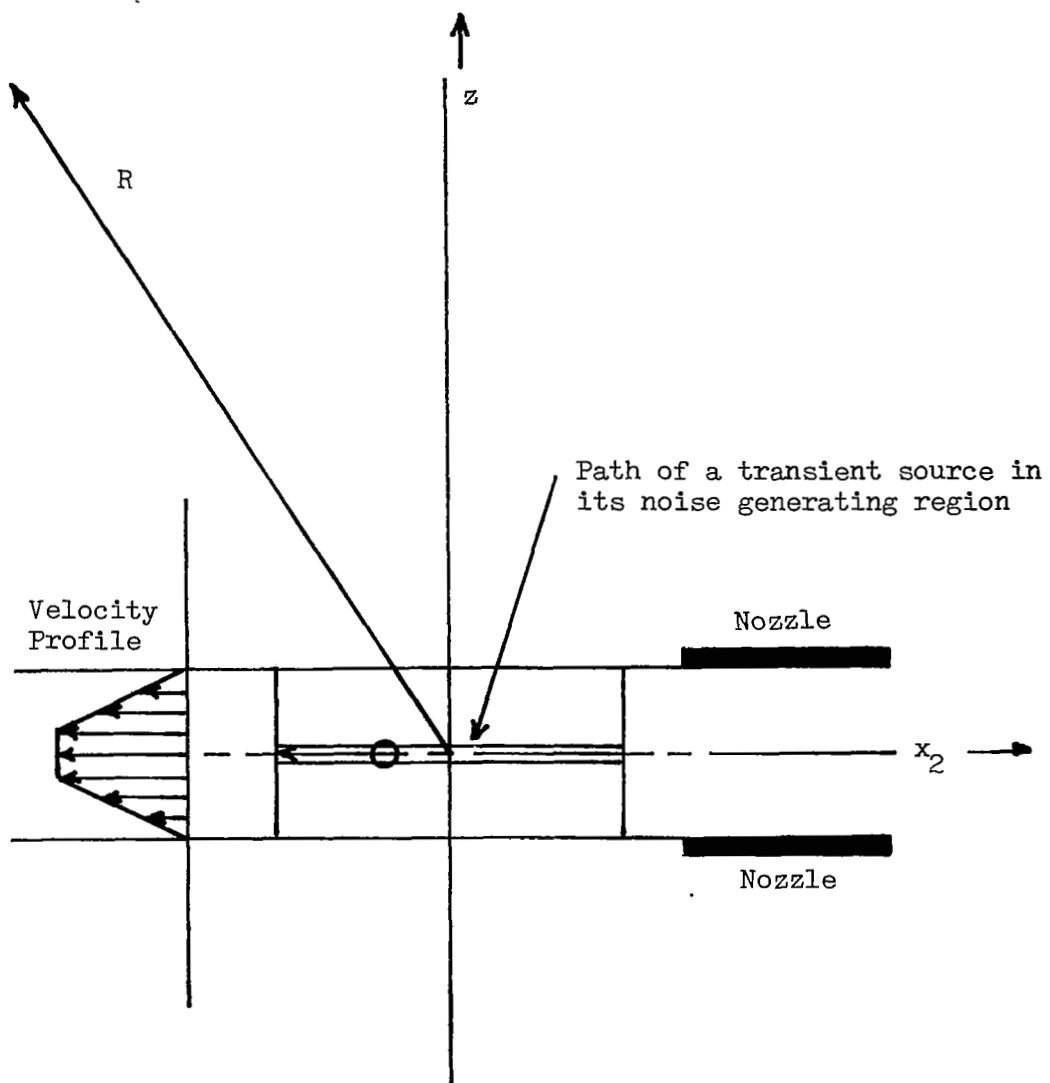
6

Fig. 2   COORDINATE SYSTEM FIXED RELATIVE TO
NOZZLE (RETARDED COORDINATES)

case if the $|1 + Mx_2/R|$ factors are enclosed by absolute magnitude signs.)

Solutions

The methods just described have been amply illustrated in previous reports[1,13,14]. Power series solutions for sources in two-dimensional shear-layer jets and in circular-cylindrical shear-layer jets are given in Ref. 1 and are not repeated here. These previously-derived solutions were programmed for machine computation and are the basis for calculating all shear-layer jet results presented in the first section of Part 1 of the present report.

The partial differential equation for the shear layer is Eq. (37) of NASA CR-2390. This should provide a good first approximation for cold jets of low supersonic Mach number, where temperature gradient effects are considerably smaller than velocity gradient effects. For high supersonic Mach numbers and heated jets it may be necessary to use Eq. (107) of CR-2390 which includes temperature gradients.

The Near Field

Near-field calculations are much more difficult than far-field calculations for two reasons. Stationary phase approximations cannot be used, and the transient sources cannot be assumed to pass through many cycles. To get a realistic picture of the near field, transient sources must generally be required to have very short lifetimes. This will be discussed further in Part 2.

Part 1   PEAKS IN THE FAR-FIELD DIRECTIVITY PATTERN FOR SUPERSONIC JETS

Introduction and Examples

In one of our first investigations of supersonic jets (see Ref. 14) the example chosen was for Mach number 3, the jet was two-dimensional and the source was located at the center of the jet. The velocity profile was a linear variation from maximum velocity at the center to zero velocity at the edge. In this case the mean-square pressure plotted against angle in the far field showed zero at the Mach angle, but showed a high finite peak in the "subsonic approach region" and a much lower peak in the "supersonic approach region". Both of these peaks were near the Mach angle. (The source Mach number of 3 projected onto any angular ray gives an "approach" Mach number of 3 or less for that ray. When the approach Mach number is less than unity we say the far field point is in the subsonic approach region. When the approach Mach number is greater than unity the far field point is said to be in the supersonic approach range of angles.)

This result seemed reasonable. The cruder representation of the jet by stationary fluid with "moving sources" passing through it shows an infinite (and unrealistic) peak at the Mach angle. The requirement that jet fluid must move with the sources (as in the present analysis) apparently produces a more realistic result.

However the consideration of an _off-center_ source in the jet described above (a more difficult problem) produced an unexpected result. Fig. 3 shows the effect of locating the source one-quarter of the way from the centerline to the edge of the jet. The source, drifting with the local fluid in the shear layer, now travels at a Mach number of 2.25 . The expected and comparatively broad peaks in the subsonic and supersonic approach regions are much lower than before and now there appears a "spike" confined to less than one degree of angular range but hundreds of times higher than the other peaks. In an ordinary survey of the far
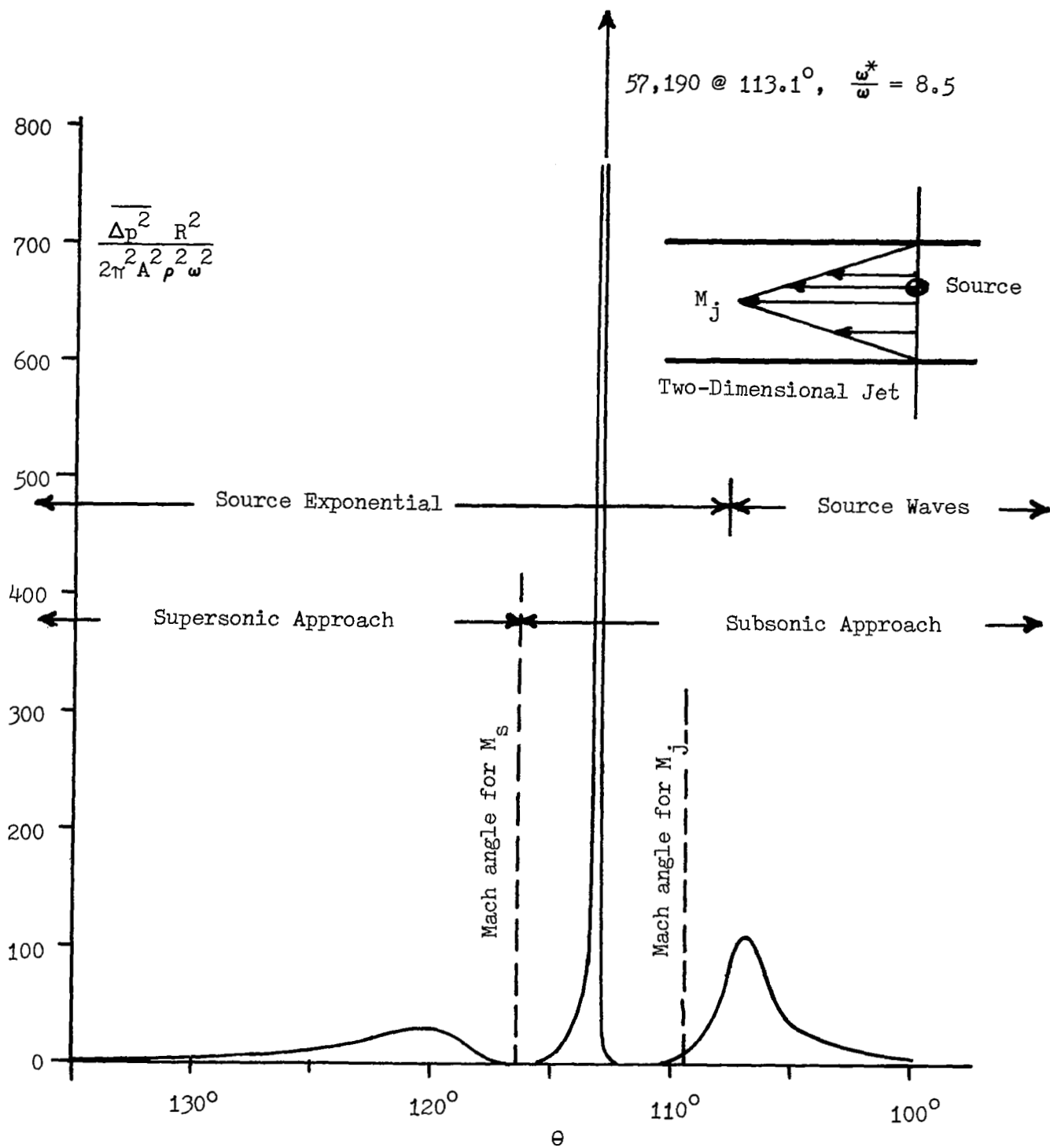
Fig. 3   "SPIKE" IN FAR-FIELD MEAN-SQUARE PRESSURE FROM SOURCES
IN SHEAR LAYER OF TWO-DIMENSIONAL SUPERSONIC JET
$(M_j = 3.0, \quad M_s = 2.25, \quad S_T = 0.2)$

10

field with a five-degree angle interval, or even a one-degree interval, such an effect might be completely overlooked. It is not yet known whether the area under such a spike would contribute significantly to the final integrated results.

Studies were also made of two-dimensional jets at a Mach number of 1.5 . In Fig. 4 mean-square pressure is plotted against far-field angle for a jet whose velocity profile is linear, giving M = 1.5 at the center and M = 0 at the edge. The source is at the center. A high peak appears in the subsonic approach region as in the M = 3 case, and the supersonic approach peak is negligible (see Fig. 5). For a second case we let the jet have uniform velocity over the central half of the jet thickness, then velocity decreasing linearly to zero at the edge. The source is located halfway between the center and the edge, and so its Mach number is 1.5 as in the preceding case. However the subsonic approach peak is now greatly reduced (see Fig. 4) and a supersonic approach peak of similar magnitude appears (see Fig. 5). Such effects are not easily explained. In a third example the source is located in the shear layer, three-quarters of the way from the centerline to the edge. This source, drifting with the fluid, travels at M = 0.75 . There is of course no supersonic approach region based on source Mach number, and the mean-square pressure plot somewhat resembles the subsonic jet type as might be expected (see Fig. 6).

We now turn our attention to circular cylindrical jets with M = 1.5 . In each case the jet has a central core traveling at uniform velocity (corresponding to M = 1.5), and an annular region in which the velocity varies linearly from the central value to zero at the outer edge of the jet. The radius of the central region is $\bar{r}_0$, and the radius at which the source is located is $\bar{r}_s$. The mean-square pressure is an average value obtained by integrating around the jet. In Figs. 7 and 8 results are shown for a variety of values of core radius, the source being located either at the center or at the edge of the core. Thus the source, drifting with the fluid always travels at M = 1.5. In Fig. 7 the subsonic approach region is shown. The subsonic approach peak is highest for the smallest central core, and decreases rapidly as the core size is increased.
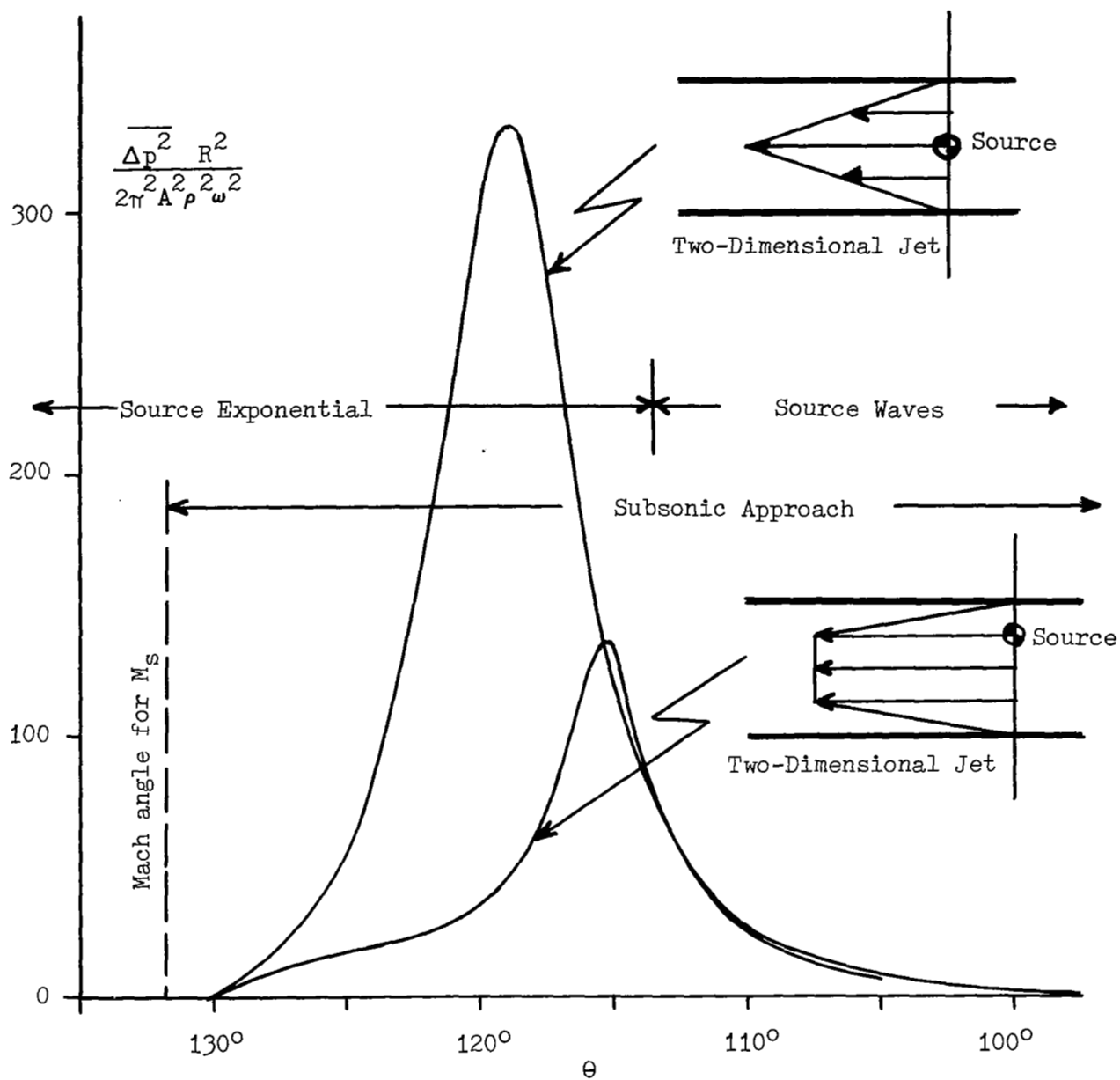
Fig. 4 EFFECT OF VELOCITY PROFILE ON FAR-FIELD MEAN-SQUARE PRESSURE
FOR SOURCES IN TWO-DIMENSIONAL SUPERSONIC JET
(Subsonic Approach Angles, $M_s = M_j = 1.5$, $S_T = 0.2$)
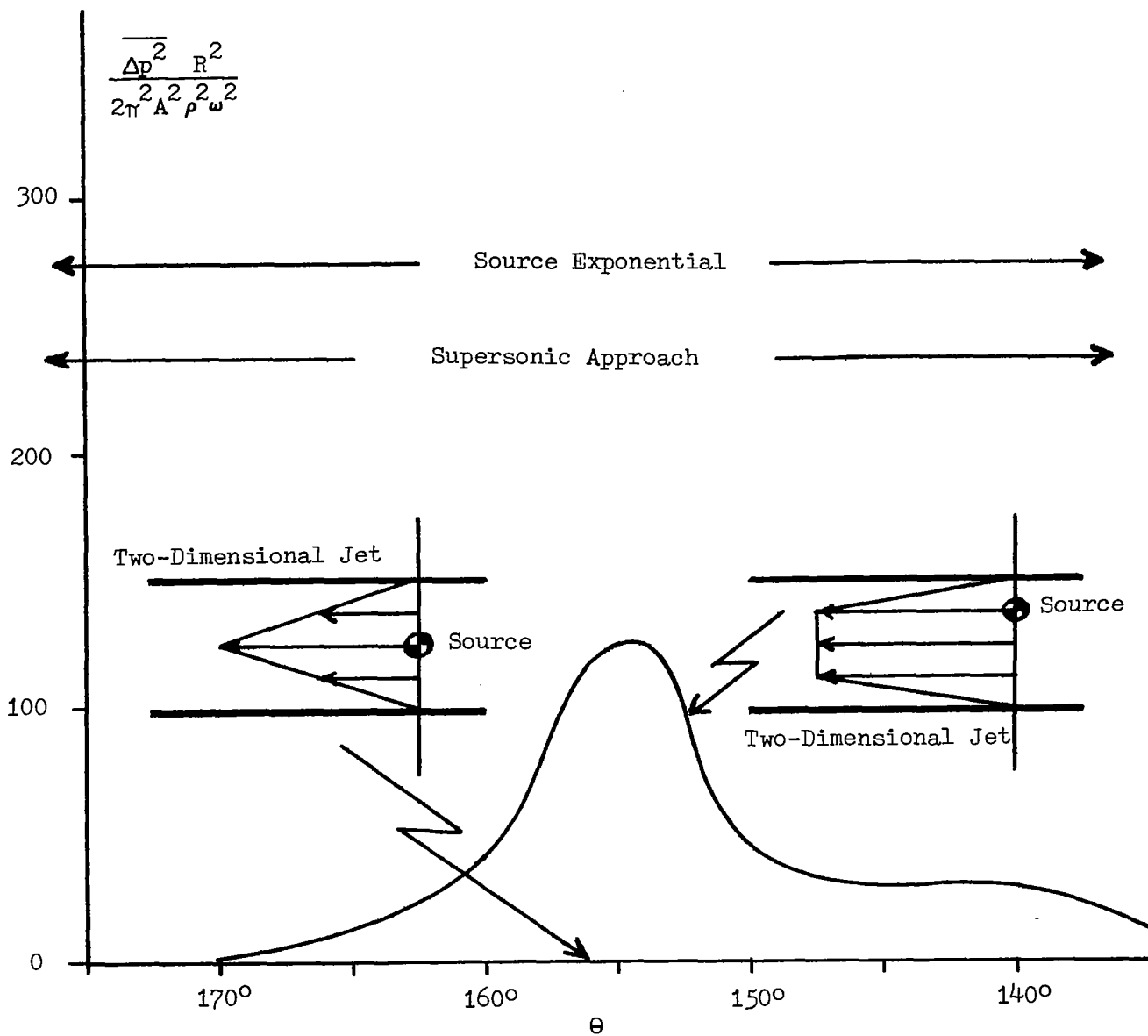
Fig. 5   EFFECT OF VELOCITY PROFILE ON FAR-FIELD MEAN-SQUARE PRESSURE
FOR SOURCES IN TWO-DIMENSIONAL SUPERSONIC JET
(Supersonic Approach Angles, $M_S = M_j = 1.5$, $S_T = 0.2$)
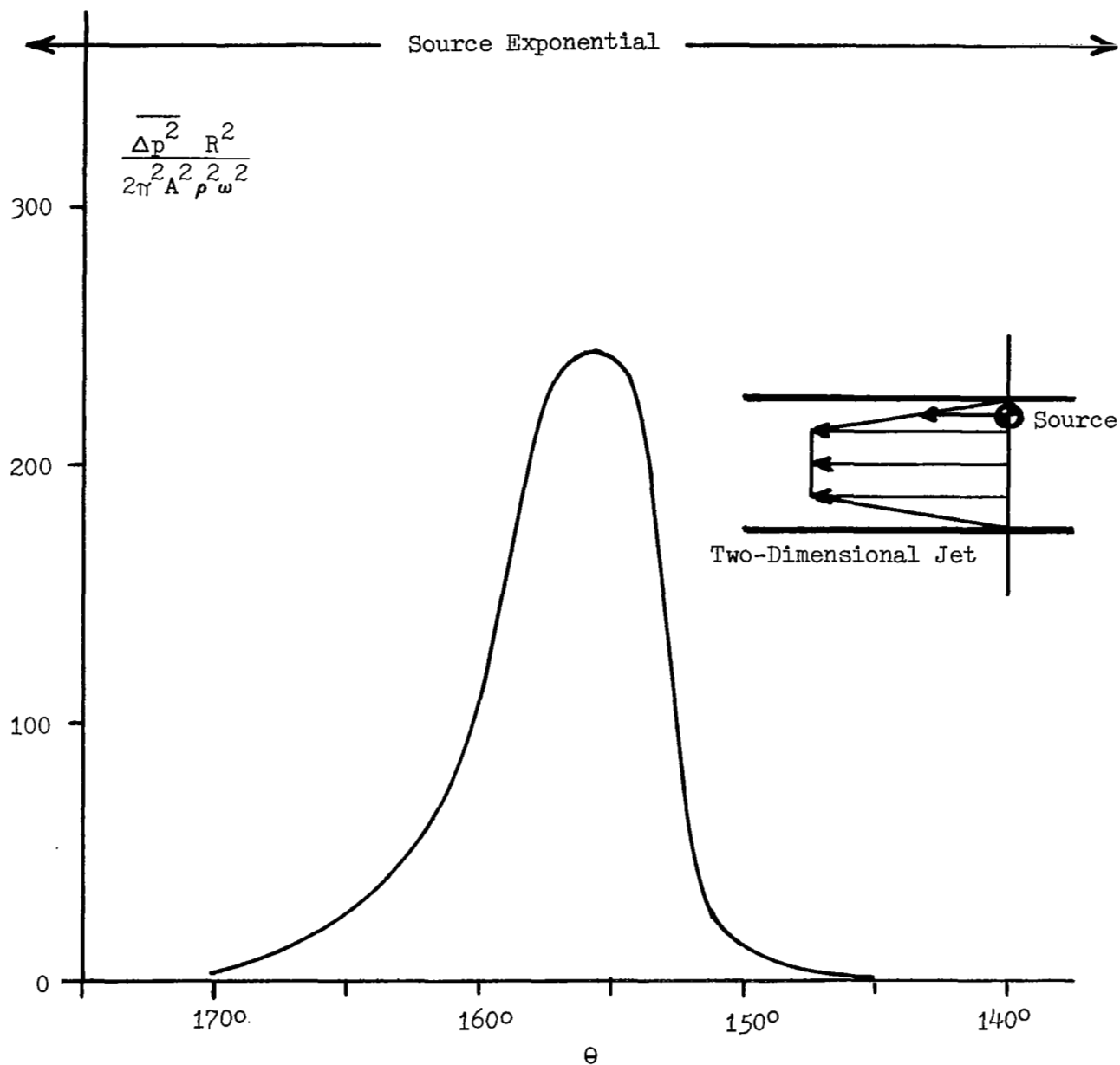
Fig. 6   FAR-FIELD MEAN-SQUARE PRESSURE FROM SOURCES IN
SHEAR LAYER OF TWO-DIMENSIONAL SUPERSONIC JET
$(M_j = 1.5, \quad M_s = 0.75, \quad S_T = 0.2)$

14

Fig. 7 FAR-FIELD MEAN-SQUARE PRESSURE FROM SOURCES IN THE
CENTRAL REGION OF A SUPERSONIC CIRCULAR JET
(<u>Subsonic</u> Approach Angles, $M_s = M_j = 1.5$, $S_T = 0.2$)

15

Fig. 8   FAR-FIELD MEAN-SQUARE PRESSURE FROM SOURCES IN THE
CENTRAL REGION OF A SUPERSONIC CIRCULAR JET
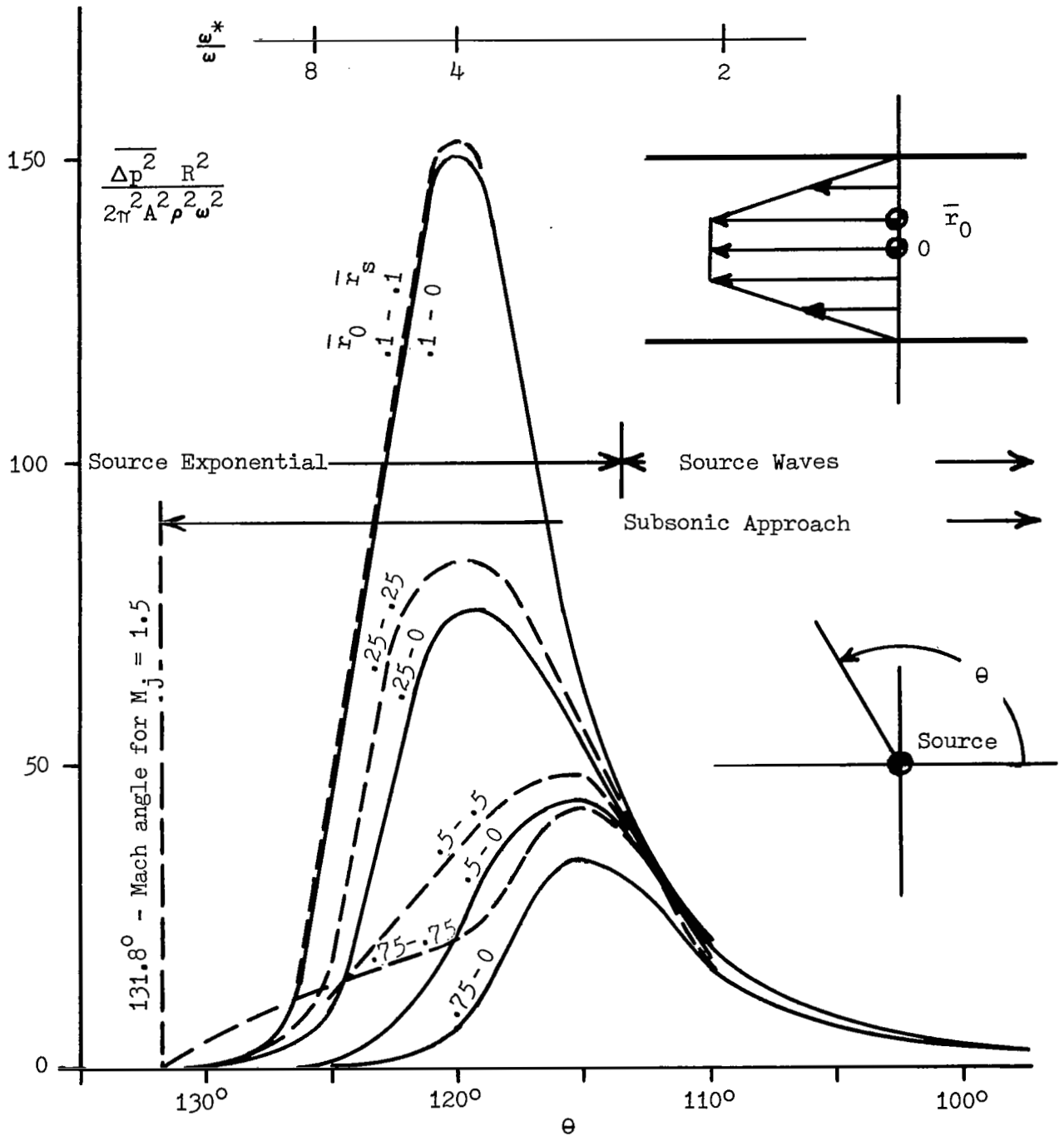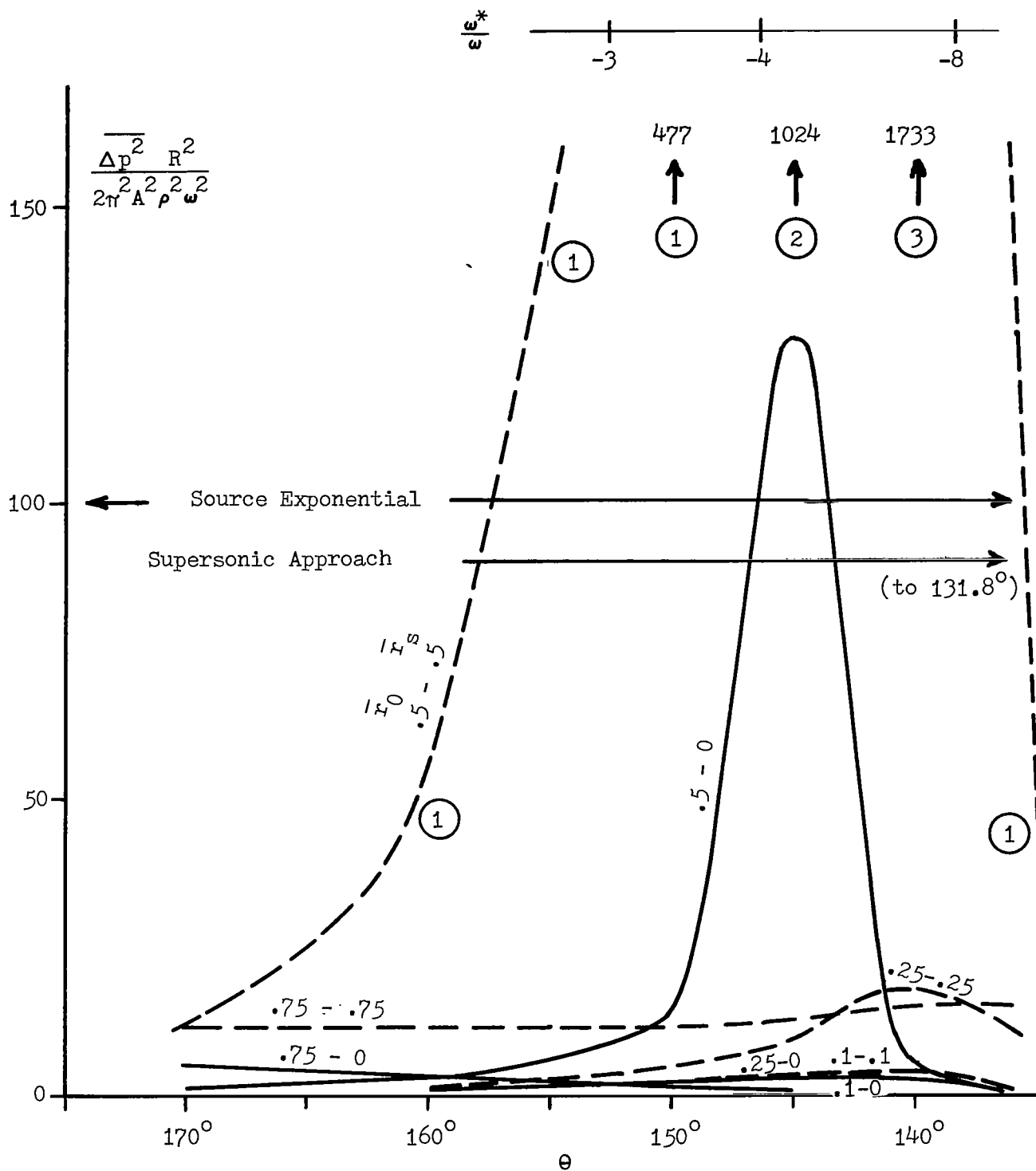(Supersonic Approach Angles, $M_s = M_j = 1.5$, $S_T = 0.2$)

In fig. 8 the supersonic approach region is shown. It is necessary at this point to explain that a source at radius $\bar{r}_s$ and angle $\psi = 0$ in the jet is constructed by the Fourier series representation of a delta-function. The first term is a uniform distribution of source strength on the circle of radius $\bar{r}_s$. The next term is a simple cosine ψ term, the next a cosine 2ψ term, etc., each with the appropriate coefficient to represent a delta-function. Since the wavelength created by the pulsating source is generally much greater than $2\bar{r}_s$ we expected the zero harmonic to behave much like a simple source, the first harmonic like a dipole, etc. Each higher harmonic would then have a much smaller contribution to the mean-square pressure than the preceding one. In many cases this turned out to be correct, and convergence was rapid. However Fig. 8 shows for $\bar{r}_0 = \bar{r}_s = 0.5$ a very high peak due largely to the third harmonic*. This is a rather surprising result. Presumably it is produced by some sort of quasi-resonant effects associated with communication around the jet. Such effects would not appear in the two-dimensional examples. However the "spikes" occurring in two-dimensional examples also occur for the circular jet, though perhaps more rarely. For $\bar{r}_0 = \bar{r}_s = 0.45$, $S_T = 0.2$, $M_j = 1.5$ (see Fig. 9) a spike was encountered in the supersonic approach region. This very high peak was contained within an angular range of one degree or less.

In the examples just considered the source was either at the center or at the edge of the core, traveling at a Mach number of 1.5. In Fig. 10 we show for several core radii the effect of locating a source in the shear layer just far enough out so that it travels at $M = 0.7$. For jets with larger cores the sources will then be nearer the outer edge of the jet, but all sources travel at the same Mach number. It is interesting that the peaks vary widely in position and magnitude, showing the extreme importance of jet velocity profile in modifying the radiation pattern of sources convected at a specified velocity. It is also of interest that the mean-square pressures are nearly zero at the Mach angle

---

*Where they are of interest dominant harmonics are noted on the curves by a 0, 1, 2, 3 etc. enclosed in a circle.
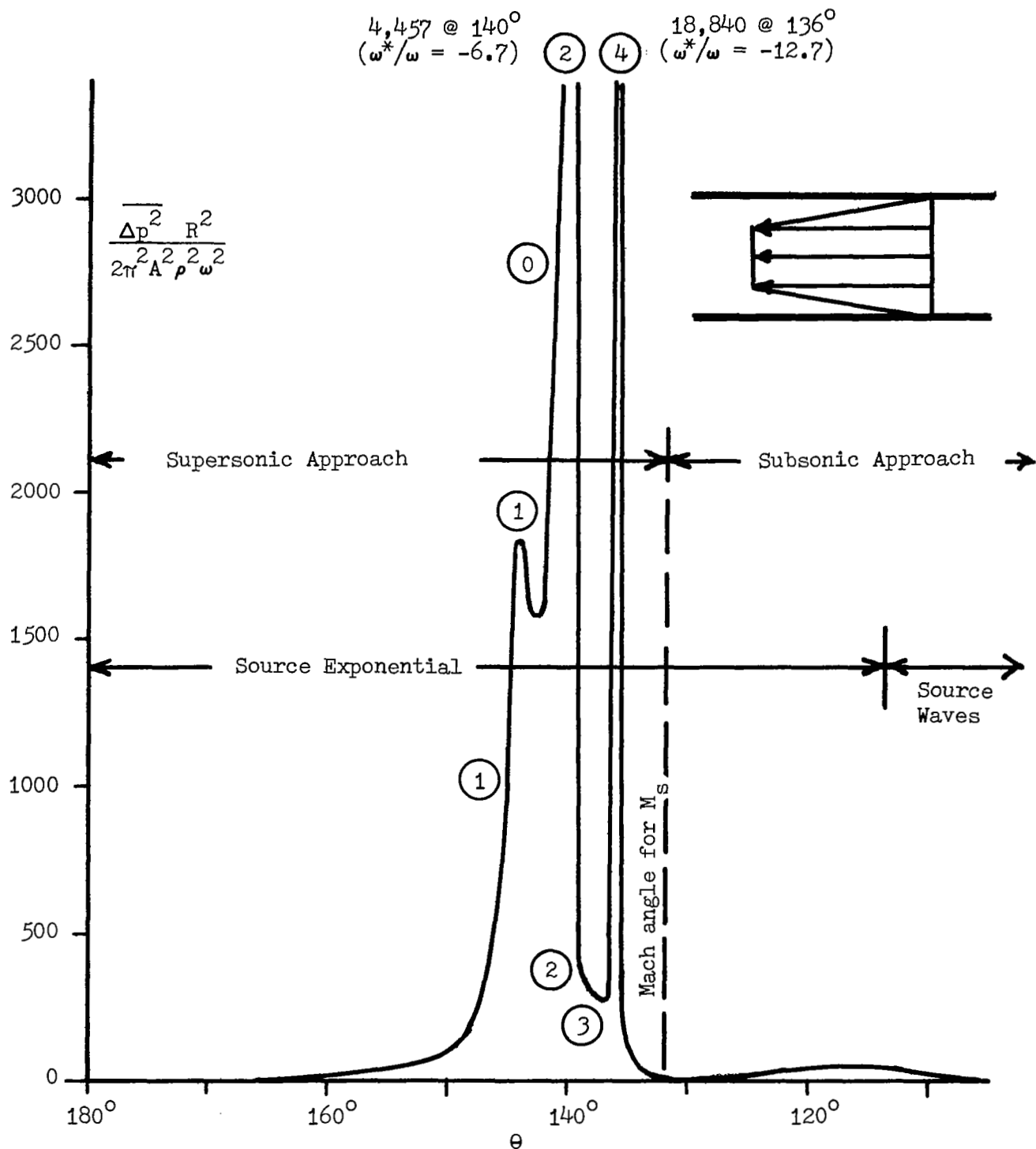
Fig. 9   "SPIKES" IN FAR-FIELD MEAN-SQUARE PRESSURE FROM SOURCES
IN THE CENTRAL REGION OF A SUPERSONIC CIRCULAR JET

$$(M_j = M_s = 1.5, \quad \bar{r}_0 = \bar{r}_s = 0.45)$$

18

$$\frac{\overline{\Delta p^2}\ R^2}{2\pi^2 A^2 \rho^2 \omega^2}$$

300 — Source Exponential —

200

r_0 r_s
.5 - .77

2

2

100

1

.75 - .88

.25 - .65

.1 - .58

131.8° – Mach angle for M_j = 1.5
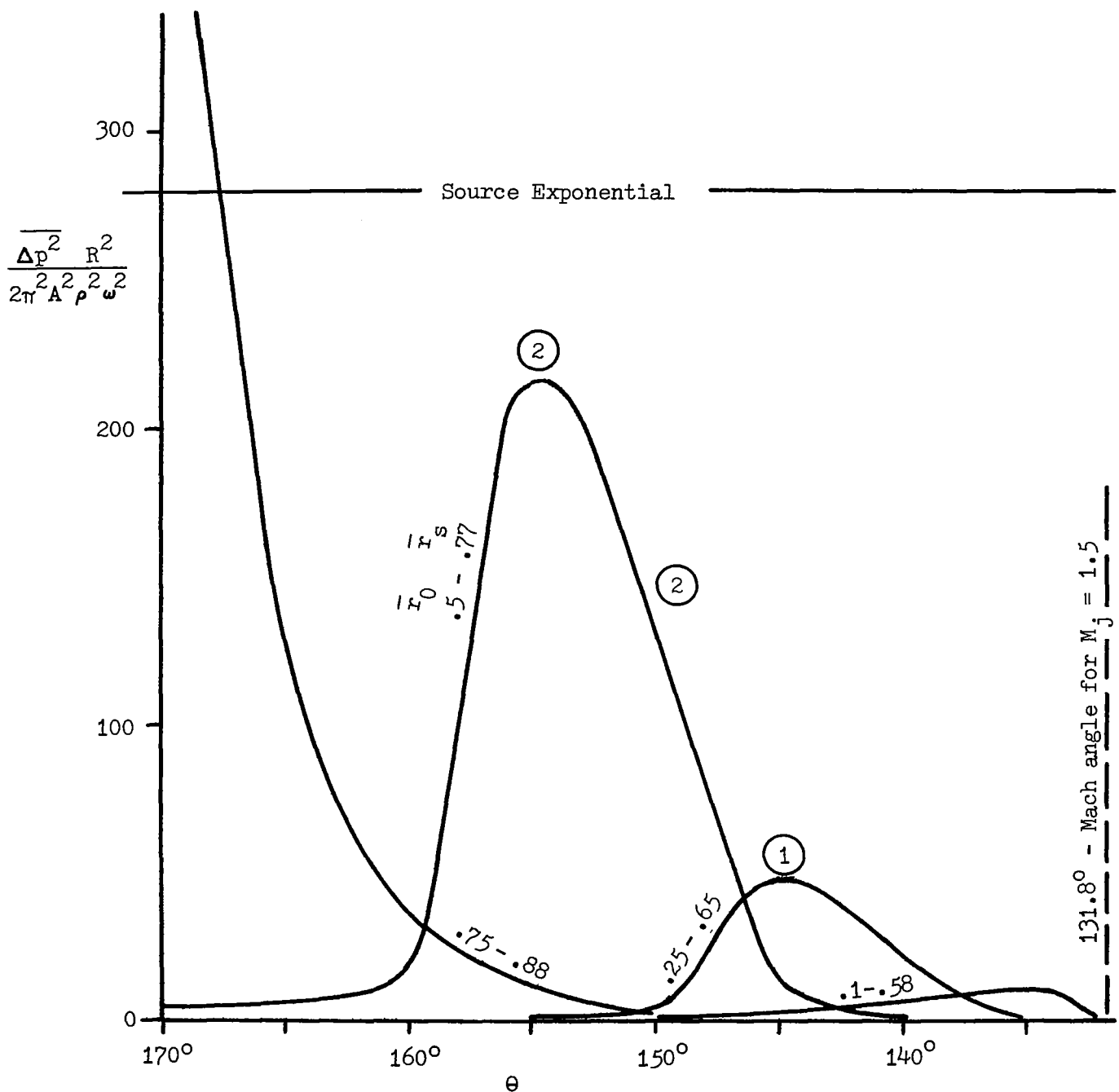
0

170°   160°   150°   140°

θ

Fig. 10   FAR-FIELD MEAN-SQUARE PRESSURE FROM SOURCES AT M_s = 0.7

IN SHEAR LAYER OF SUPERSONIC CIRCULAR JET

(M_j = 1.5, S_T = 0.2)

19

corresponding to the _jet_ Mach number even though the source velocity
is subsonic.

Figures 11 and 12 show the radiation patterns when the sources are
so placed in the shear layer that M_s = 0.5 and 0.3 . The mean-square
pressures are much lower in general, because of the lower convection
speeds. The extreme effects of velocity profile are still apparent, and
some double peaks now appear. For angles less than 131.8° mean-square
pressures are not negligible, but are not of special interest here.

In view of the unexpected and rather perplexing results of the
supersonic jet analysis it seemed desirable to get a check on the
correctness of the basic formulation of the problem and on the computa-
tions. The following two sections are devoted to the independent study
of simplified models of two-dimensional and circular jets.

The Three Layer Model of the Two-Dimensional Jet

This case is particularly valuable in giving an understanding of
spikes because it can be studied analytically to a large extent and
the necessary numerical calculations can be made with a small computer
(e.g. the HP-35).

The model is illustrated in Fig. 13 and the analysis follows the
general procedure outlined in the introduction. The absence of a shear
layer of course simplifies that procedure.

The velocity potential in any region, ⓪, ① or ②, satisfies
the simple wave equation

$$\nabla^2 \phi = \frac{1}{c^2} \phi_{tt} \tag{1}$$

for coordinates at rest in the fluid of that region. Only outgoing
waves need be considered in the ambient air, and for simplicity the
analysis given here treats only ordinary waves (i.e. $K_1 M_1 < 1$, subsonic
approach angles), though note is made of the changes required for the
reversed wave case ($K_1 M_1 > 1$, supersonic approach angles). For simplicity,

20

Fig. 11   FAR-FIELD MEAN-SQUARE PRESSURE FROM SOURCES AT M_s = 0.5
IN SHEAR LAYER OF SUPERSONIC CIRCULAR JET
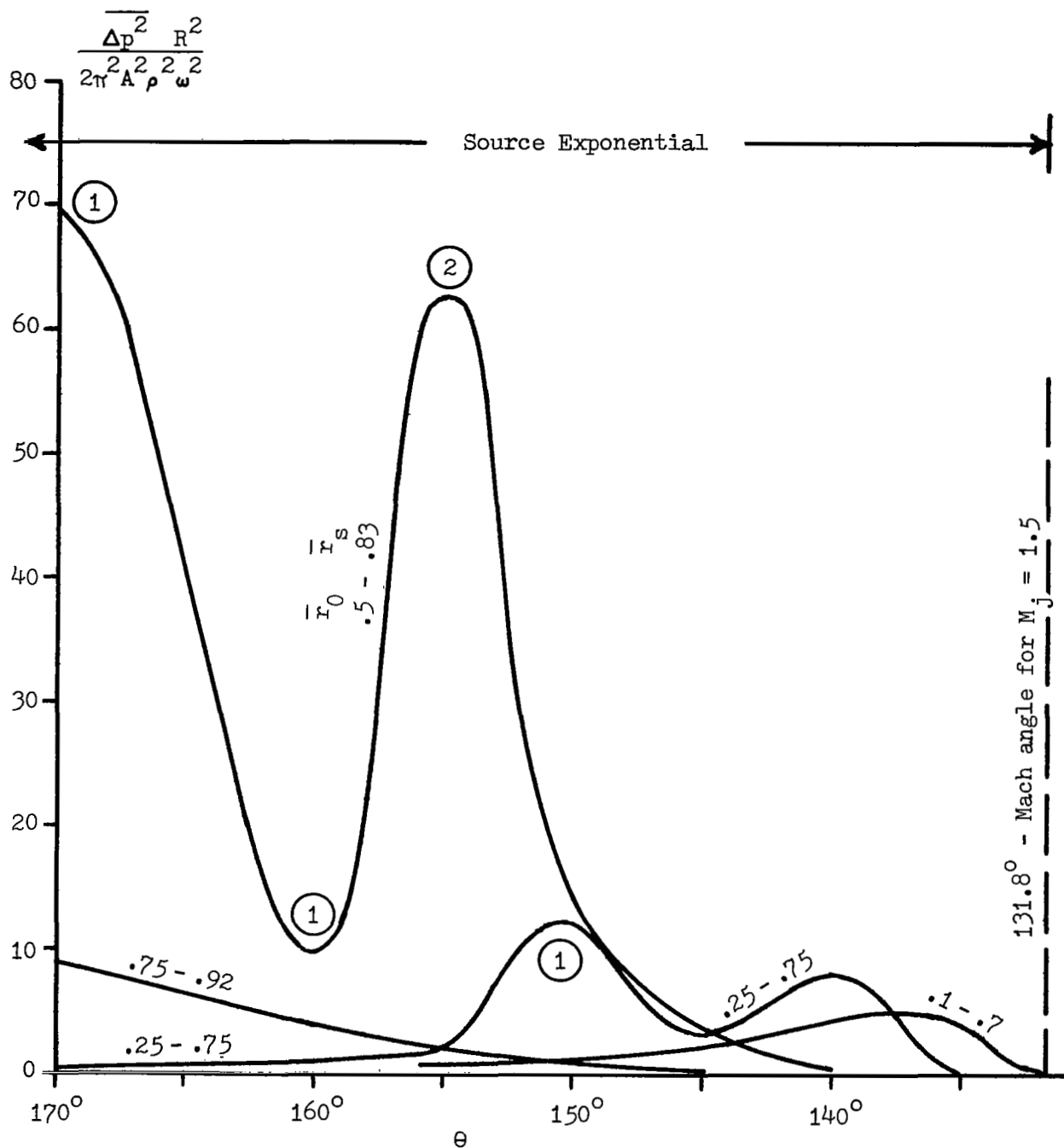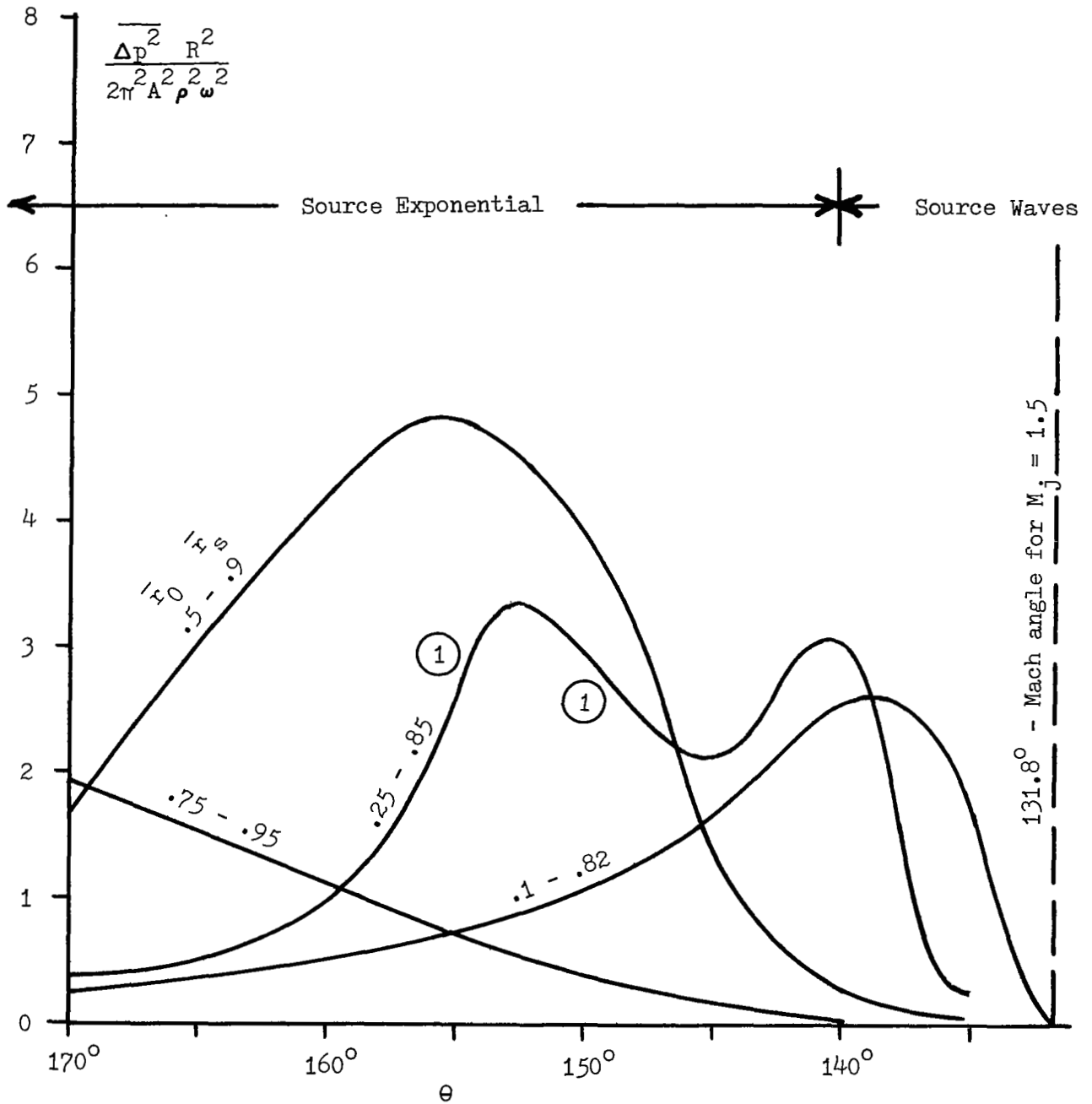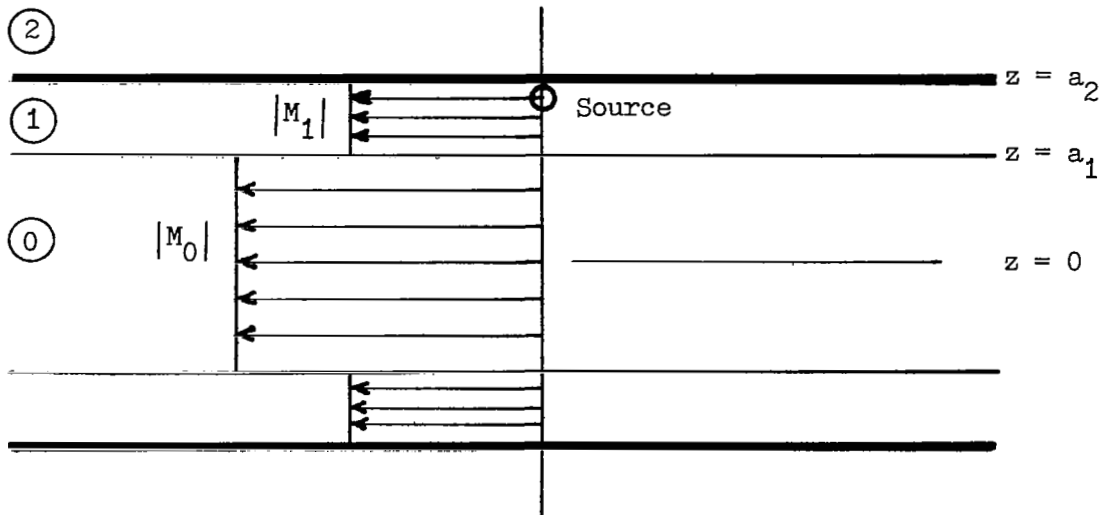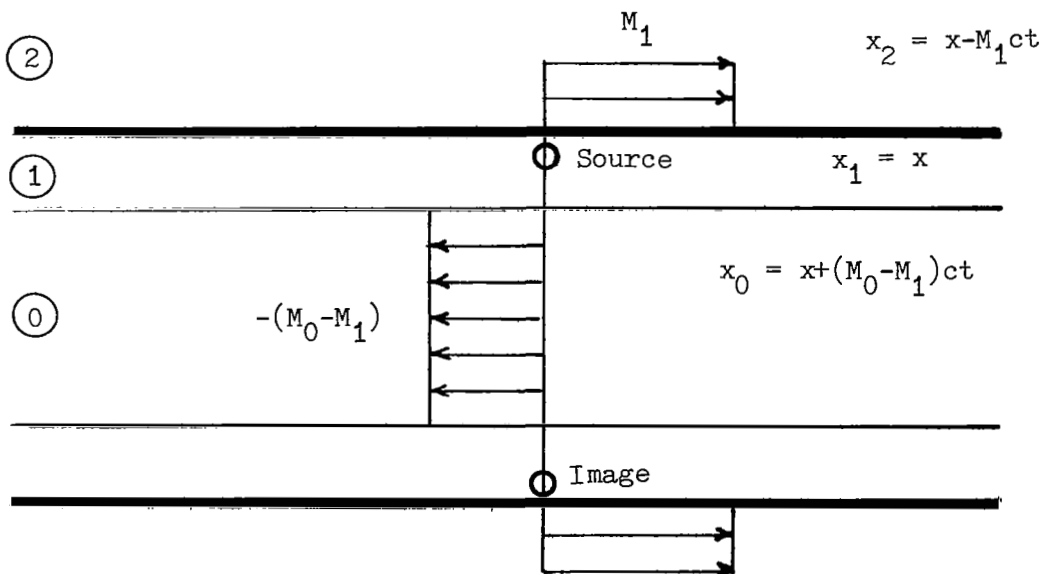
$(M_j = 1.5, \quad S_T = 0.2)$

21

Fig. 12   FAR-FIELD MEAN-SQUARE PRESSURE FROM SOURCES AT M_s = 0.3

IN SHEAR LAYER OF SUPERSONIC CIRCULAR JET

$(M_j = 1.5,   S_T = 0.2)$

(a)   Geometry and Velocity Profile

(b)   Velocity Profile for Coordinates Fixed in the Source

Fig. 13   THE THREE LAYER MODEL OF THE TWO-DIMENSIONAL JET

also, we consider a symmetric problem (source at z_s and image source at $-z_s$) and an anti-symmetric problem (source at z_s and "sink", i.e. 180° out-of-phase source, at $-z_s$) and write equations only for $z > 0$. The solution for the single source at $z = z_s$ is then the superposition of a symmetric solution and an anti-symmetric solution, each of half-strength.

For this example the source is situated in the outer layer. The potentials in the three regions (Fig. 13b) may then be expressed as

$$\Delta\phi_0 = A\omega' \text{ R.P. } \bar{R}\left[\exp\left\{i\omega'\left(K_1[x_0-(M_0-M_1)ct]+K_2y-ct+z\sqrt{[1+(M_0-M_1)K_1]^2-K^2}\right)\right\}\right.$$
$$\left. \pm \exp\left\{i\omega'\left(K_1[x_0-(M_0-M_1)ct]+K_2y-ct-z\sqrt{[1+(M_0-M_1)K_1]^2-K^2}\right)\right\}\right] \quad (2)$$

$$\Delta\phi_1 = A\omega' \text{ R.P. } \left[\exp\left\{i\omega'[K_1x+K_2y-ct+|z-z_s|\sqrt{1-K^2}]\right\}/\sqrt{1-K^2}\right.$$

$$+ \bar{B} \exp\left\{i\omega'[K_1x+K_2y-ct+z\sqrt{1-K^2}]\right\}$$

$$+ \left. \bar{D} \exp\left\{i\omega'[K_1x+K_2y-ct-z\sqrt{1-K^2}]\right\}\right] \quad (3)$$

$$\Delta\phi_2 = A\omega' \text{ R.P. } \bar{S} \exp\left\{i\omega'[K_1(x_2+M_1ct)+K_2y-ct+(z-a_2)\sqrt{(1-M_1K_1)^2-K^2}]\right\} \quad (4)$$

where R.P. denotes "real part of" and the complex notation is convenient. In these equations A is the source strength coefficient [A = (source strength)/$8\pi^2$, the source strength being the maximum volume introduced per unit time]; $\bar{B}, \bar{D}, \bar{R}, \bar{S}$ are unknown complex amplitude coefficients to be determined. In $\Delta\phi_1$ the first term is the component potential due to the point source; the other two terms are upward-moving and downward-moving reflected waves. In $\Delta\phi_0$ the upper sign applies to the symmetric problem described above and the lower sign applies to the anti-symmetric problem. $\Delta\phi_0$ thus is chosen to satisfy required conditions of symmetry or anti-symmetry at $z = 0$ (zero normal velocity, $\Delta\phi_{0_z}$, in the symmetric case; zero pressure, $-\rho\Delta\phi_{0_t}$, in the anti-symmetric case). K_1 and K_2 are reduced wave numbers ($K_1 = k_1/\omega'$, $K_2 = k_2/\omega'$, where

$\omega' = \omega/c$). $K = \sqrt{K_1{}^2 + K_2{}^2}$. $\Delta\phi_0$, $\Delta\phi_1$, $\Delta\phi_2$ are <u>component</u> potentials, of course, the total potential in each region being the integral over all positive K_1 and K_2 of the component potentials shown. (In the reversed wave case, the term involving the square-root in the exponential of $\Delta\phi_2$ changes sign, so the exponent becomes

$$\left\{ i\omega'\left[K_1(x_2 + M_1 ct) + K_2 y - ct - (z - a_2)\sqrt{(1 - M_1 K_1)^2 - K^2} \right] \right\}.)$$

The boundary conditions require matching at each interface the pressures (on the two sides of the interface) and the displacements. These four conditions determine the four amplitude coefficients $\bar{B}$, $\bar{D}$, $\bar{R}$, $\bar{S}$. The last of these is particularly of interest in describing the disturbance which is transmitted outside the jet:

$$\bar{S} = \frac{2[\ ]_N}{(1 - M_1 K_1)\sqrt{1 - K^2}\ [\ ]_D} \tag{5}$$

where

$$[\ ]_N = \left[e^{i\xi}\left(e^{i\alpha}(\mu_2 + 1) \mp e^{-i\alpha}(\mu_2 - 1) \right) \right.$$
$$\left. - e^{-i\xi}\left(e^{i\alpha}(\mu_2 - 1) \mp e^{-i\alpha}(\mu_2 + 1) \right) \right]_N \tag{6}$$

$$[\ ]_D = \left[e^{i\sigma}(\mu_1 - 1)\left(e^{i\alpha}(\mu_2 + 1) \mp e^{-i\alpha}(\mu_2 - 1) \right) \right.$$
$$\left. - e^{-i\sigma}(\mu_1 + 1)\left(e^{i\alpha}(\mu_2 - 1) \mp e^{-i\alpha}(\mu_2 + 1) \right) \right]_D \tag{7}$$

and where

$$\xi = \omega'(z_s - a_1)\sqrt{1 - K^2}$$
$$\sigma = \omega'(a_2 - a_1)\sqrt{1 - K^2}$$
$$\alpha = \omega' a_1 \sqrt{(1 + [M_0 - M_1]K_1)^2 - K^2} \tag{8}$$
$$\mu_1 = \frac{\sqrt{(1 - M_1 K_1)^2 - K^2}}{(1 - M_1 K_1)^2 \sqrt{1 - K^2}}$$
$$\mu_2 = \frac{\sqrt{(1 + [M_0 - M_1]K_1)^2 - K^2}}{(1 + [M_0 - M_1]K_1)^2 \sqrt{1 - K^2}}$$

Again, the upper sign applies to the symmetric solution and the lower sign to the anti-symmetric solution. (For the reversed wave case the corresponding solutions are obtained by substituting $-\sqrt{(1-M_1K_1)^2-K^2}$ for $+\sqrt{(1-M_1K_1)^2-K^2}$ wherever it occurs.)

Application of the far-field analysis (using the principle of stationary phase) is described in previous reports[1,12,16]. The critical K-values, which alone determine $\bar{S}$ in the far field, are, in retarded coordinates,

$$K_1 = \frac{x_2/R}{1+M_1 x_2/R}$$

$$K_2 = \frac{y/R}{1+M_1 x_2/R} \tag{9}$$

where x_2, y, z (and $R = \sqrt{x_2^2+y^2+z^2}$) are the retarded coordinates fixed in the nozzle (which is assumed to be stationary in the ambient air).

From the far-field potential for a permanent source of frequency ω (the case so far considered), the far-field potential for a transient source follows by Fourier integral construction. For the transient source sequence described in the Introduction and used in previous studies[1,13,14] the mean-square pressure in the far field, assuming each transient source to go through many cycles of frequency ω_0, is[13]

$$\overline{\Delta p^2} = \frac{2\pi^2 A^2 \rho^2 \omega_0^2}{R^2} \frac{z^2}{R^2} \frac{S'^2(\omega_0) + S''^2(\omega_0)}{|1+M_1 x_2/R|^5} \tag{10}$$

where $\bar{S} = S' + iS''$. For convenience the subscript 0 on the generating frequency is dropped in the remainder of this analysis.

Since the mean-square pressure in the far field is proportional to the square of the absolute value of the transmission factor $\bar{S}$, evaluated at the critical values of K_1, K_2 (Eqs. (9)), attention will be focused primarily on $|\bar{S}|^2$. Results were considered only in the plane

$y = 0$ where $K_2 = 0$ and $K = |K_1|$. We define $\Theta = 0$ in the upstream direction so that $\Theta = \cos^{-1}(x_2/R)$.

When Eqs. (5) and (10) were investigated for several numerical examples, spikes were found only when K was large $(K > 1)$ and when $(1+[M_0-M_1]K_1)^2 > K^2$; that is, spikes occur in this example in regions of the far field where the critical K-values correspond to exponential components of the source but to true wave disturbances in the central region of the jet. For this region, if we write $\xi = i\xi'$, $\sigma = i\sigma'$, $\mu_1 = -i\mu_1'$, $\mu_2 = -i\mu_2'$ (so that ξ', σ', μ_1', μ_2' are real) then

$$|\bar{S}|^2 = \frac{4}{(1-M_1K_1)^2(K^2-1)} \frac{N^2}{(D_1^2+\mu_1'^2 D_2^2)} \tag{11}$$

where, in the symmetric case,

$$
\begin{aligned}
N &= \cosh\xi' \cos\alpha - \mu_2' \sinh\xi' \sin\alpha \\
D_1 &= \sinh\sigma' \cos\alpha - \mu_2' \cosh\sigma' \sin\alpha \\
D_2 &= \cosh\sigma' \cos\alpha - \mu_2' \sinh\sigma' \sin\alpha
\end{aligned}
\tag{12}
$$

with

$$
\begin{aligned}
\sigma' &= \omega'(a_2-a_1)\sqrt{K^2-1} \\
\xi' &= \omega'(z_s-a_1)\sqrt{K^2-1} \\
\mu_1' &= \frac{\sqrt{(1-M_1K_1)^2-K^2}}{(1-M_1K_1)^2\sqrt{K^2-1}} \\
\mu_2' &= \frac{\sqrt{(1+[M_0-M_1]K_1)^2-K^2}}{(1+[M_0-M_1]K_1)^2\sqrt{K^2-1}}
\end{aligned}
\tag{13}
$$

and, in the anti-symmetric case,

$$N = \cosh\xi' \, \sin\alpha + \mu_2' \, \sinh\xi' \, \cos\alpha$$

$$D_1 = \sinh\sigma' \, \sin\alpha + \mu_2' \, \cosh\sigma' \, \cos\alpha \qquad (14)$$

$$D_2 = \cosh\sigma' \, \sin\alpha + \mu_2' \, \sinh\sigma' \, \cos\alpha$$

In this form it will be noticed that when K is large, μ_1' is small. Thus, for large K, D_1^2 is normally the dominant term of the denominator. However it is oscillatory and zeros of D_1 can occur in the symmetric case when

$$\tanh\sigma' = \mu_2' \, \tan\alpha \qquad (15a)$$

and in the anti-symmetric case when

$$\tan\alpha \, \tanh\sigma' = -\mu_2' \qquad (15b)$$

It is when the dominant term of the denominator drops to zero that sharp peaks occur in the far-field mean-square pressure distribution. For <u>very</u> large K (which according to Eq. (9) occur for supersonic values of M_1 near the corresponding Mach cone, i.e. near $\theta = \cos^{-1}(-1/M_1)$) there can be multiple solutions of Eqs.(15), and the pressure peaks are very abrupt in θ, becoming spikes. The magnitudes of the spikes are, for $\bar{S}$,

$$\bar{S} = f/\sin\theta \qquad (16)$$

and for the corresponding mean-square pressure

$$\frac{\overline{\Delta p^2} \, R^2}{2\pi^2 A^2 \rho^2 \omega^2} = \frac{f^2}{\left|1+M_1\cos\theta\right|^5} \qquad (17)$$

where, in the symmetric problem,

$$f = f_s = \frac{\cosh\xi' \, \cos\alpha - \mu_2' \, \sinh\xi' \, \sin\alpha}{\cosh\sigma' \, \cos\alpha - \mu_2' \, \sinh\sigma' \, \sin\alpha} \qquad (18)$$

28

and in the anti-symmetric problem

$$f = f_a = \frac{\cosh\xi'\ \sin\alpha + \mu_2'\ \sinh\xi'\ \cos\alpha}{\cosh\sigma'\ \sin\alpha + \mu_2'\ \sinh\sigma'\ \cos\alpha} \tag{19}$$

Two source locations are especially of interest. If the source is at the outer edge of the outer layer, then $\xi' = \sigma'$ and $f_s = f_a = 1$. Note that $\overline{\Delta p^2}$ then corresponds to that of the modified moving source[15]. If the source is at the inner edge of the outer layer, then $\xi' = 0$ and (using Eqs. (15)) $f_s = f_a = \cosh\sigma'$. The mean-square pressure in this case is much larger than that for the modified moving source (and approaches infinite value at the Mach cone for supersonic M_1).

Note also, however, that there are zeros in the symmetric problem contribution to the far-field pressure distribution when

$$\tanh\xi'\ \tan\alpha = 1/\mu_2' \tag{20a}$$

and in the anti-symmetric contribution when

$$\tan\alpha = -\mu_2'\ \tanh\xi' \tag{20b}$$

For very large K these zeros are not far removed (in Θ) from the spikes located according to Eqs. (15a,b).

Further examination of Eq. (5) reveals additional information for other parts of the far field where spikes were not found.

(a) When $K^2 > 1$ and $K^2 > (1 + [M_0 - M_1]K_1)^2$, then neither term of the denominator of $|\bar{S}|^2$ is oscillatory and no spikes can occur.

(b) When $K^2 < 1$ and $K^2 \gtrless (1 + [M_0 - M_1]K_1)^2$, both terms of the denominator are oscillatory but neither is dominant (i.e. $|\mu_1| = 0(1)$). Hence, although pressure peaks may occur, their magnitude is more limited. Also, since the variation of the critical K-value with Θ (location in the far field) is not rapid for those Θ where $K < 1$, there are no real

spikes. Pressure peaks occur singly and with moderate slope (in plots of $\overline{\Delta p^2}$ vs. θ).

This example illustrates the type of problem encountered when the supersonic shear-layer jets were investigated. For the shear-layer jets abrupt spikes sometimes occurred in the numerical solution, as illustrated earlier. For all cases checked, the spikes were associated with the sudden vanishing of one term of the denominator, a term which dominated the denominator at nearby θ's. These spikes existed over less than a degree in θ, so that they could easily be overlooked in any but an extremely fine survey of the far-field. The question then arises whether it is possible to predict that section (or sections) of the far field where spikes might be expected and whether one can know when all of the spikes have been located for a given problem. The very simple example being considered here, where the jet shear layers are replaced by two constant-velocity layers on either side of a central layer of higher constant velocity, shows some of the difficulties of answering this question.

For this example, the three-layer model of the two-dimensional jet, the following generalities probably can be made:

(a) Spikes occur only when $K_1^2 > 1$. (This appears to be true also for shear-layer jets.) Now, in general,

$$K_1 = \frac{\cos\theta}{1 + M_1 \cos\theta}$$

so that if M_1 is subsonic $(M_1 < 1)$

$$\pi \geqslant \theta \geqslant 0 \quad \text{corresponds to} \quad -\frac{1}{1-M_1} < K_1 \leqslant \frac{1}{1+M_1} \tag{21a}$$

and if $M_1 > 1$

$$\pi \geqslant \theta > \cos^{-1}(-1/M_1) \quad \text{corresponds to} \quad \frac{1}{M_1+1} \geqslant K_1 > -\infty$$

$$\cos^{-1}(-1/M_1) > \theta \geqslant 0 \quad \text{corresponds to} \quad \infty > K_1 \geqslant \frac{1}{M_1-1} \tag{21b}$$

(See Fig. 14-a.)

(b) The possibility of spikes requires that $\sqrt{(1+[M_0-M_1]K_1)^2-K^2}$

be real. If $(M_0-M_1) < 1$ this happens for

$$- \frac{1}{1+(M_0-M_1)} \leqslant K_1 \leqslant \frac{1}{1-(M_0-M_1)} \tag{22a}$$

and if $(M_0-M_1) > 1$ it requires

$$- \infty < K_1 \leqslant - \frac{1}{(M_0-M_1)-1} \;;\; - \frac{1}{(M_0-M_1)+1} \leqslant K_1 < \infty \tag{22b}$$

(See Fig. 14-b.)

Thus, if (M_0-M_1) is subsonic and M_1 is subsonic, there is no overlapping of the K_1-ranges of Eq. (21a) and Eq. (22a) such that $K_1^2 > 1$, and no spikes can occur.

If $M_1 < 1$ and $(M_0-M_1) > 1$ there will be an overlapping of the K_1-ranges of Eq. (21a) and (22b) in a region where $K_1^2 > 1$ if

$$- \frac{1}{1-M_1} < - \frac{1}{(M_0-M_1)-1}$$

This requires

$$M_0 > 2$$

(M_0 is the jet center-region Mach number.) Note that the overlapping K_1-range is finite, so there can be relatively few peaks, if any. Also, although $K_1^2 > 1$, it is not excessively large and the magnitude of the peaks is therefore limited. Since the phase change of α (Eq. (8)) is limited in the overlapping K_1-range, it is not difficult to numerically locate all of the peaks in this case, using Eqs. (15).

If $M_1 > 1$ and $(M_0-M_1) < 1$ there will again be overlapping of the pertinent K_1-ranges (Eq. (21b) and Eq. (22a)) when $K_1^2 > 1$ if

$$\frac{1}{M_1-1} < \frac{1}{1-(M_0-M_1)}$$

(a) $M_1 < 1$

$(1-K_1M_1)^2 = K^2$

$K = 1$

$K_1 = -\frac{1}{1-M_1}$

$K_1 = \frac{1}{1+M_1}$

K_2

K_1

(b) $M_1 > 1$

$(1-K_1M_1)^2 = K^2$

$K = 1$

$(1-K_1M_1)^2 = K^2$

$K_1 = \frac{1}{M_1+1}$

$K_1 = \frac{1}{M_1-1}$

K_2
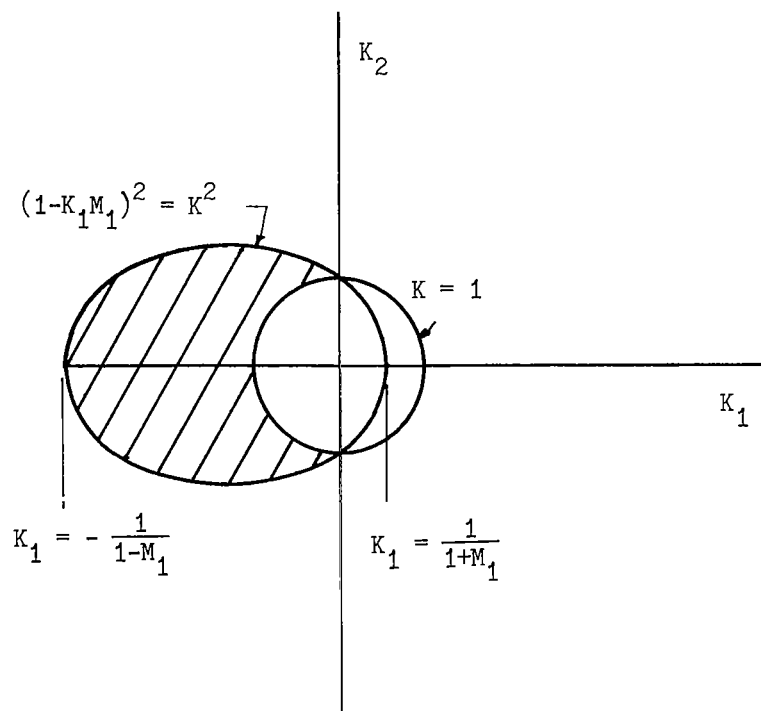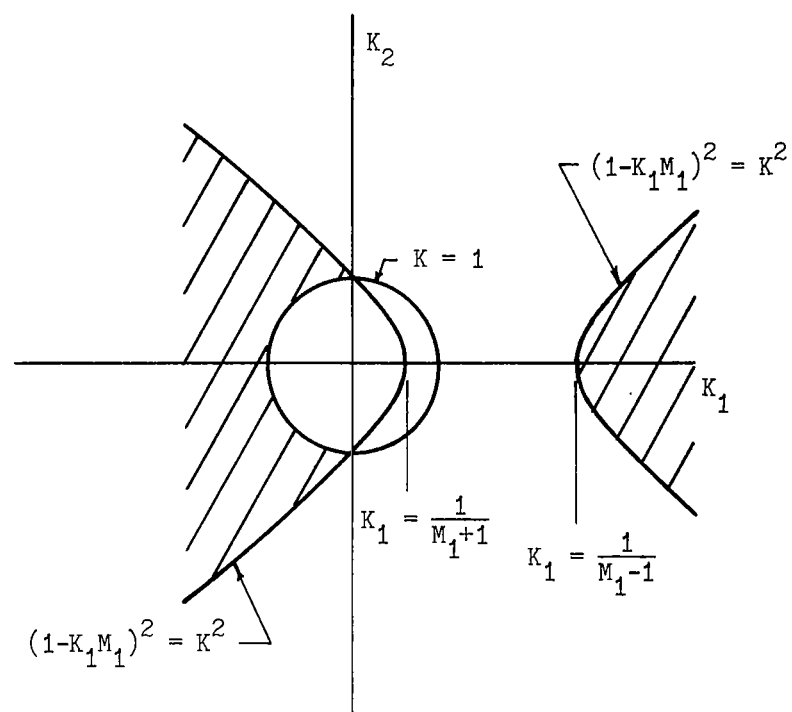
K_1

Fig. 14-a   REGIONS OF THE K-PLANE CORRESPONDING TO $2\pi > \theta > 0$ AND $K^2 > 1$

$$\left[1+(M_0-M_1)K_1\right]^2 = K^2$$

$$\left[1+(M_0-M_1)K_1\right]^2 = K^2$$

$K = 1$

K_2

K_1

$$K_1 = -\frac{1}{1+(M_0-M_1)}$$

$$K_1 = \frac{1}{1-(M_0-M_1)}$$

$$\left[1+(M_0-M_1)K_1\right]^2 = K^2$$

$$K_1 = -\frac{1}{(M_0-M_1)-1}$$

$K = 1$

K_2

K_1

$$K_1 = -\frac{1}{(M_0-M_1)+1}$$

(a) $(M_0-M_1) < 1$

(b) $(M_0-M_1) > 1$

33
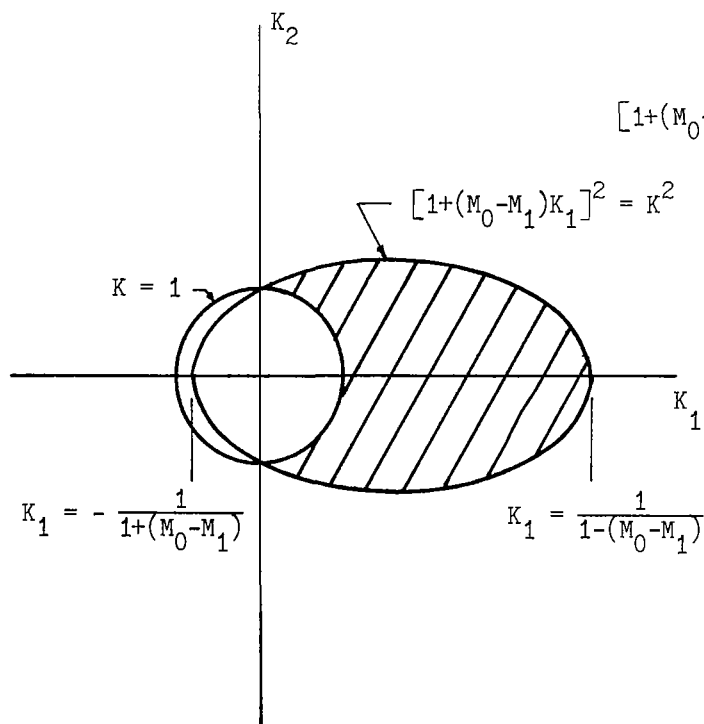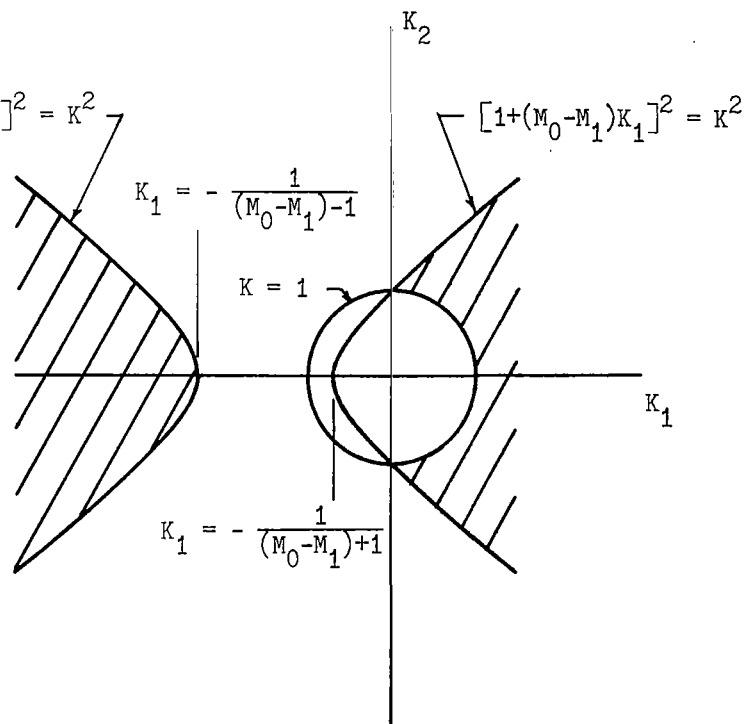
Fig. 14-b   REGIONS OF THE K-PLANE CORRESPONDING TO α REAL AND $K^2 > 1$

Again this leads to the requirement $M_0 > 2$. Again the peaks are limited in number and somewhat limited in magnitude.

Finally, if both $M_1 > 1$ and $(M_0-M_1) > 1$ there is overlapping of the K_1-ranges of Eq. (21b) and Eq. (22b) for

$$K_1 < -\frac{1}{(M_0-M_1)-1} \quad \text{and} \quad K_1 > \frac{1}{M_1-1}$$

(Of course, if $(M_0-M_1) > 2$, we are interested only in $K_1 < -1$ on the negative side, and if $M_1 > 2$ we are interested only in $K_1 > 1$ on the positive side, in order to stay within the $K_1^2 > 1$ criterion.) Since $|K_1|$ is unlimited in this case, the number of possible peaks is infinite and the magnitude of the spikes can get very large when $|K_1| \to \infty$ (that is, when $\theta \to \cos^{-1}(-1/M_1)$, the Mach angle corresponding to the source velocity). Note also that the spacing (in θ) between the spikes diminishes continually as $|K_1| \to \infty$.

We repeat that all of our calculations have been made for the plane $y = 0$ in this two-dimensional problem, so that $K_2 = 0$, $K = |K_1|$ (from Eqs. (9)). If K_2 is not zero, that is $y \neq 0$, the foregoing conclusions probably can be extended to the appropriate overlapping regions of the K_1, K_2 plane (see Fig. 14). The criteria for locating spikes are less simply written in such cases, but appear to be straightforward enough. However, if the shear layer of the jet were to be approximated by _multiple_ layers, each introducing phase-changing quantities similar to α, σ used above, it will be foreseen that the criteria for the possible existence of spikes become very complicated indeed.

Analysis similar to the preceding has been carried out for the three-layer two-dimensional jet when the source is located in the central high-velocity layer of the jet. In this case no spikes were found in the far-field pressure distributions of any of the examples investigated. This result appears to follow from the fact that, although the denominator of the transmission factor $|\overline{S}|^2$ is the sum of two oscillatory terms, neither one is truly dominant in any K_1-range (that is, in any θ-range).

The Circular-Cylindrical Jet Having Two Constant-Velocity Layers

This model consists of a cylindrical central region having constant high velocity, surrounded by an annular layer having smaller constant velocity. Viewed in any section containing the axis of the jet, the velocity distribution appears the same as previously sketched for the corresponding two-dimensional model. Fig. 15 shows the velocity distribution and the parameters used to describe the two-layered circular cylindrical jet.

This model, like the previous one, has also the advantage that an analytical solution can be obtained. Because of the cylindrical functions involved, however, and because an off-center source is represented mathematically as a series of such functions, numerical calculations for specific examples are considerably lengthier than for the two-dimensional case. A survey of the far-field pressure distribution for any example would be formidable without the aid of a programmed computer.

In cylindrical coordinates the velocity potential for a source which is at rest with respect to the immediately surrounding fluid and which is located at r_s, ψ_s may be written

$$\phi_s = \pi A \omega' \sum_{n=0}^{\infty} \epsilon_n \cos[n(\psi-\psi_s)] \text{ R.P.} \int_{-\infty}^{\infty} e^{i\omega'(Kx-ct)} \cdot$$

$$\cdot J_n(r_s\omega'\sqrt{1-K^2}) H_n^{(1)}(r\omega'\sqrt{1-K^2}) \, dK ; \quad (r > r_s)$$

or   (23)

$$\phi_s = \pi A \omega' \sum_{n=0}^{\infty} \epsilon_n \cos[n(\psi-\psi_s)] \text{ R.P.} \int_{-\infty}^{\infty} e^{i\omega'(Kx-ct)} \cdot$$

$$\cdot J_n(r\omega'\sqrt{1-K^2}) H_n^{(1)}(r_s\omega'\sqrt{1-K^2}) \, dK ; \quad (r < r_s)$$

(A is the source strength factor previously defined; $\omega' = \omega/c$ where c is the speed of sound; $K = k/\omega'$ where k is wave number in the x-
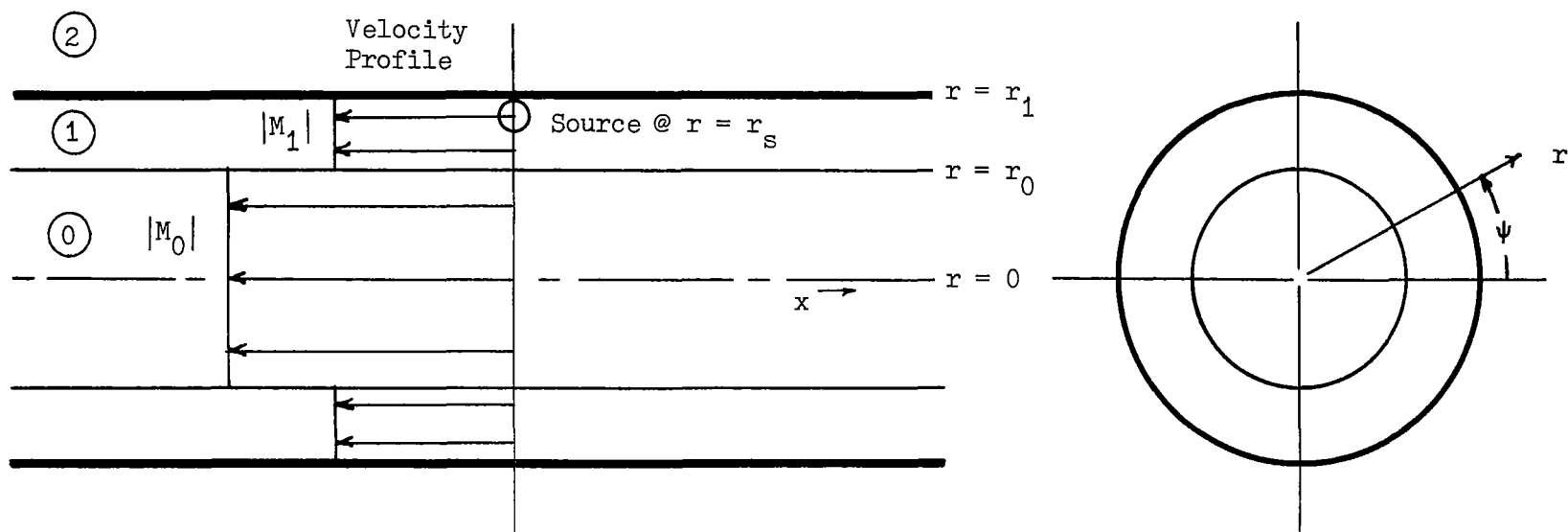
Fig. 15   THE CIRCULAR CYLINDRICAL JET HAVING TWO CONSTANT-VELOCITY LAYERS

direction; $\epsilon_0 = 1$, $\epsilon_n = 2$ for $n = 1,2,3,\cdots$; $J_n(\ )$, $H_n^{(1)}(\ )$ are cylindrical functions, basic solutions of the Bessel equation.) For convenience we write the source potential as

$$\phi_s = \text{R.P.} \sum_{n=0}^{\infty} \int_{-\infty}^{\infty} \phi_{s_n}(K)\ dK \tag{24}$$

where $\phi_{s_n}(K)$ is the component source potential for one wave number pair (K,n) . (In what follows we will write only component potentials for the various regions, it being understood that the total potential is obtained from the component by integrating over all K (positive and negative) and summing over n (zero plus all positive integers).)

In each of the three regions shown in Fig. 15 the velocity potential satisfies the wave equation (in cylindrical coordinates) for coordinates at rest in the fluid of that region. With the source located in the outer annulus of the jet we can write

(a) for region $\boxed{0}$ $(0 < r < r_0)$ (See Fig. 15) :

$$\phi_{0_n} = \pi A \omega'\ \epsilon_n\ \cos[n(\psi - \psi_s)]\ \text{R.P.}\left[\ \bar{R}_n\ \exp\{i\omega'[K\{x_0 - (M_0 - M_1)ct\} - ct]\}\right.$$

$$\left. \cdot\ J_n(r\omega'\sqrt{(1+[M_0 - M_1]K)^2 - K^2})\ \right] \tag{25}$$

(b) for region $\boxed{1}$ $(r_0 < r < r_1)$:

$$\phi_{1_n} = \phi_{s_n} + \pi A\omega'\ \epsilon_n\ \cos[n(\psi - \psi_s)]\ \text{R.P.}\left[\ \exp\{i\omega'(Kx - ct)\}\ \cdot\right.$$

$$\left. \cdot\ \left[\ \bar{E}_n\ H_n^{(1)}(r\omega'\sqrt{1-K^2})\ +\ \bar{G}_n\ H_n^{(2)}(r\omega'\sqrt{1-K^2})\ \right]\ \right] \tag{26}$$

(c) for region ② $(r > r_1)$:

$$\phi_{2_n} = \pi A \omega' \, \epsilon_n \, \cos\left[n(\psi-\psi_s)\right] \; \text{R.P.}\left[\bar{S}_n \, \exp\left\{i\omega'\left[K(x_2+M_1 ct)-ct\right]\right\}\right. \cdot$$

$$\left. \cdot \; H_n^{(1)}\left(r\omega'\sqrt{(1-M_1 K)^2-K^2}\right)\right] \qquad (27)$$

(When $(1-M_1 K)^2 > K^2$ and $K > (1/M_1)$, $H_n^{(1)}\left(r\omega'\sqrt{(1-M_1 K)^2-K^2}\right)$ is

replaced by $H_n^{(2)}\left(r\omega'\sqrt{(1-M_1 K)^2-K^2}\right)$; this is the "reversed wave" region[12], and the change to Hankel functions of the second kind preserves out-going waves as required for the solution outside the jet.)

Satisfaction of boundary conditions of equal pressure and equal displacement on either side of the boundaries at $r = r_0$ and at $r = r_1$ permits evaluation of the complex amplitude coefficients $\bar{R}_n$, $\bar{E}_n$, $\bar{G}_n$, $\bar{S}_n$.

Using the following convenient definitions

$$\sigma_0 = \omega' r_0 \sqrt{1-K^2}$$

$$\sigma_1 = \omega' r_1 \sqrt{1-K^2}$$

$$\sigma_s = \omega' r_s \sqrt{1-K^2}$$

$$\lambda = \omega' r_0 \sqrt{\left(1+[M_0-M_1]K\right)^2-K^2} \qquad (28)$$

$$\eta = \omega' r_1 \sqrt{(1-M_1 K)^2-K^2}$$

$$\mu_1 = \frac{\sqrt{(1-M_1 K)^2-K^2}}{(1-M_1 K)^2 \sqrt{1-K^2}}$$

$$\mu_2 = \frac{\sqrt{\left(1+[M_0-M_1]K\right)^2-K^2}}{\left(1+[M_0-M_1]K\right)^2 \sqrt{1-K^2}}$$

the transmission coefficient $\bar{S}_n$ for the cylindrical layered jet is

$$\bar{S}_n = \frac{4i}{\pi\sigma_1(1-M_1K)} \quad \frac{J_n(\sigma_s)\ [\ ]_{N_{1n}} - H_n^{(1)}(\sigma_s)\ [\ ]_{N_{2n}}}{[\ ]_{D_n}} \tag{29}$$

where

$$[\ ]_{N_{1n}} = J_n(\lambda)\, H_n^{(1)'}(\sigma_0) - \mu_2\, J_n'(\lambda)\, H_n^{(1)}(\sigma_0)$$

$$[\ ]_{N_{2n}} = J_n(\lambda)\, J_n'(\sigma_0) - \mu_2\, J_n'(\lambda)\, J_n(\sigma_0) \tag{30}$$

$$[\ ]_{D_n} = \left[J_n(\lambda)\, H_n^{(2)'}(\sigma_0) - \mu_2\, J_n'(\lambda)\, H_n^{(2)}(\sigma_0) \right] \cdot$$

$$\cdot \left[H_n^{(1)}(\eta)\, H_n^{(1)'}(\sigma_1) - \mu_1\, H_n^{(1)'}(\eta)\, H_n^{(1)}(\sigma_1) \right]$$

$$- \left[J_n(\lambda)\, H_n^{(1)'}(\sigma_0) - \mu_2\, J_n'(\lambda)\, H_n^{(1)}(\sigma_0) \right] \cdot$$

$$\cdot \left[H_n^{(1)}(\eta)\, H_n^{(2)'}(\sigma_1) - \mu_1\, H_n^{(1)'}(\eta)\, H_n^{(2)}(\sigma_1) \right]$$

(Note again that, in the reversed wave region $H_n^{(1)}(\eta)$ and its derivative $H_n^{(1)'}(\eta)$ are replaced by $H_n^{(2)}(\eta)$, $H_n^{(2)'}(\eta)$.)

The far-field analysis, the change to a transient source sequence (instead of a permanent source) and to retarded coordinates then follow in the manner indicated in previous studies[1,14]. As shown in Ref. 1 (Eq. (95)), the <u>average</u> mean-square pressure in the far field due to a ring of random-phase transient sources (of many cycles duration) located at $r = r_s$ is

$$\frac{\overline{\Delta p^2}\, R^2}{2\pi^2 A^2 \rho^2 \omega^2} = \frac{1}{|1+M_1\cos\theta|^3} \sum_{n=0}^{\infty} \epsilon_n(S_n'^2 + S_n''^2) \tag{31}$$

where S_n', S_n'' are evaluated at the critical value of K which for a point x_2, R in the far field is

$$K = \cos\theta/(1+M_1\cos\theta) \tag{32}$$

$(\theta = \cos^{-1}x_2/R \ , \quad R = \sqrt{x_2^2+r^2} \ ; \quad \bar{S}_n = S_n' + iS_n'' \ ).$

To discover peaks we would examine $|\bar{S}_n|^2 = S_n'^2 + S_n''^2$. For the region $K^2 > 1$, $(1+[M_0-M_1]K)^2 > K^2$, for example, Eq. (30) leads to

$$|\bar{S}_n|^2 = \frac{4}{(\pi\omega'r_1)^2(1-M_1K)^2(K^2-1)} \ \frac{N_n^2}{(D_{1_n}^2 + D_{2_n}^2)} \tag{33}$$

where

$$N_n = I_n(\sigma_s') \left[J_n(\lambda) K_n'(\sigma_0') - \mu_2' J_n'(\lambda) K_n(\sigma_0') \right]$$

$$- K_n(\sigma_s') \left[J_n(\lambda) I_n'(\sigma_0') - \mu_2' J_n'(\lambda) I_n(\sigma_0') \right]$$

$$\tag{34}$$

$$D_{1_n} = \left[J_n(\lambda) K_n'(\sigma_0') - \mu_2' J_n'(\lambda) K_n(\sigma_0') \right] \ \cdot$$

$$\cdot \left[J_n(\eta) I_n'(\sigma_1') - \mu_1' J_n'(\eta) I_n(\sigma_1') \right]$$

$$- \left[J_n(\lambda) I_n'(\sigma_0') - \mu_2' J_n'(\lambda) I_n(\sigma_0') \right] \ \cdot$$

$$\cdot \left[J_n(\eta) K_n'(\sigma_1') - \mu_1' J_n'(\eta) K_n(\sigma_1') \right]$$

$$D_{2_n} = \left[J_n(\lambda) K_n'(\sigma_0') - \mu_2' J_n'(\lambda) K_n(\sigma_0') \right] \ \cdot$$

$$\cdot \left[Y_n(\eta) I_n'(\sigma_1') - \mu_1' Y_n'(\eta) I_n(\sigma_1') \right]$$

$$- \left[J_n(\lambda) I_n'(\sigma_0') - \mu_2' J_n'(\lambda) I_n(\sigma_0') \right] \ \cdot$$

$$\cdot \left[Y_n(\eta) K_n'(\sigma_1') - \mu_1' Y_n'(\eta) K_n(\sigma_1') \right]$$

with $\sigma_0 = i\sigma_0'$, $\sigma_1 = i\sigma_1'$, $\sigma_s = i\sigma_s'$, $\mu_1 = -i\mu_1'$, $\mu_2 = -i\mu_2'$ so that σ_0', σ_1', σ_s', μ_1', μ_2' are real. (Primes on the Bessel functions $\left[J_n{}'(\ ),\ Y_n{}'(\ ),\ I_n{}'(\ ),\ K_n{}'(\ ) \right]$ indicate a derivative with respect to the argument; i.e. $I_n{}'(\sigma_1') = \left[\dfrac{d}{d\sigma'}\, I_n(\sigma') \right]_{\sigma'=\sigma_1'}$, etc.)

Although D_{1_n} and D_{2_n} both are oscillatory, it is not obvious that either one is dominant in some K-range (nor that it at the same time has one or more zeros within that K-range). Such a situation may occur, but it is probably much less frequent than in the corresponding two-dimensional case studied previously.

In the limited number of numerical examples investigated, no spikes in the mean-square pressure distributions were found. Even for these examples, however, it is not clear that spikes do not occur at all. The far-field survey may simply have over-looked them by using too-large Θ-increments. (Preliminary inspection of computed results indicates that this is probably the case, the calculations showing denominator factors that oscillate very rapidly and with wide amplitude variation as Θ changes, in some instances.) These examples did show important harmonic effects. That is, for Θ-values where K is large, the primary contribution to mean-square pressure, from Eq. (31), did not come from the $n = 0$ source-strength harmonic alone; contributions of approximately equal magnitude often were made by the first several harmonics.

General Discussion of Peaks

The preceding sections indicate that the peaks or "spikes" appearing in plots of mean-square pressure versus angle for supersonic jets are not the result of numerical errors or computational difficulties, nor are they the result of convergence problems in series solutions for the shear layer. Instead they constitute a real part of the theoretical results. (Also, the lower and broader double peaks produced by harmonic effects in the circular jet appear to be real.)

It has already been suggested that the spikes are quasi-resonant

effects, and in Appendix A a drastically simplified model is shown to exhibit both resonant and quasi-resonant effects. (A denominator passing through zero to give an infinite peak corresponds to resonance. The dominant part of a denominator passing through zero to give a finite peak corresponds to quasi-resonance.)

The two-dimensional layer model, which can be studied analytically, offers a much better method for investigating peaks (see earlier sub-section). For this model only sources in the outer layers create peaks, and these occur only when there are exponential-type disturbances in the outer layers and true waves in the inner layer (exponential-wave). The three other cases (wave-wave, exponential-exponential and wave-exponential) do not produce peaks. (The disturbances outside the jet must of course always be true waves if they are to persist into the far field.)

The peaks occur near the Mach angle for the source Mach number, and in some cases there may be infinitely many peaks. The observed frequencies are generally high, approaching infinity at the source Mach angle. The peaks themselves are finite (except precisely at the source Mach angle in the layer model case) and always occur when the dominant one of two denominator terms passes through zero.

When the sources are at the outer edges of the outer layers the peak values of mean-square pressure are the same as those produced by "modified moving sources"[15], designated "point volume displacement sources by Mani[5] and by Morfey and Tanna[9].

Experimental observations in the far field of a supersonic jet would probably never reveal "spikes". Such observations include the effects of many sources having different positions, velocities and frequencies, and the smoothing produced by this inevitable "integration" should conceal any spikes. For the same reason a mathematical integration over frequency (e.g. that required to represent a transient source of short lifetime) should eliminate spikes in the final theoretical results. However this does not remove the numerical difficulties in precisely defining the shapes of spikes contributing to the final smoothed result.

Only if the areas under the spikes were negligible (compared to the area under the remainder of the mean-square pressure vs. θ curve) would the difficulties vanish, and this has not been investigated.

It has been noted that the spikes seem to occur at high observed frequencies. For example, in Figs. 3 and 9 the observed frequencies are 8.5, 6.7, and 12.7 times the generating frequency*. The simplest way to avoid numerical difficulties created by spikes is to exclude the higher ranges of observed frequency. This is not inconsistent with experimental approaches since the radiated energy in the far field is often recorded for several observed frequency bands.

To pursue this idea further one might attempt to plot far-field mean-square pressure versus angle for prescribed observed frequencies (or observed frequency bands). However this requires the assumption of source intensity as a function of generating frequency. (A fixed observed frequency is produced by one generating frequency at one angle and by a different generating frequency at another angle.) Such an assumption might require extensive investigation.

Heating the jet can have the effect of reducing the probability of encountering spikes in the pressure distribution since for fixed velocity the local Mach number (based on local temperature) is then reduced. This is illustrated in Appendix B for the simplified three-layer two-dimensional jet model when each layer has a constant temperature higher than ambient.

----

* The Strouhal number is 0.2 based on generating frequency, local jet velocity (at jet center) and local jet diameter. The Strouhal numbers based on observed frequencies are then 1.7, 1.34 and 2.54.

CONCLUSIONS - Part 1

1.   Two unexpected features appear in plots of mean-square pressure vs. angle in the far field for supersonic jets when sources are moved off center. First, "spikes" (very high, very narrow peaks) are found near the Mach angle for the source for two-dimensional jets and, to a lesser extent, for circular jets. Second, for circular jets, lower and broader multiple peaks appear. These are associated with harmonic effects (communication _around_ the jet).

2.   Neither of these features is the result of numerical errors or computing difficulties, nor are they the result of convergence problems in series solutions for the shear layer. Instead they appear to constitute a real part of the theoretical results for cold, low supersonic Mach number jets. However further investigation is certainly desirable to determine if the areas under the spikes are large enough to provide significant contributions to integrated results, and to consider the effect of temperature and temperature gradients (see Eq. (107) of NASA CR-2390[1]) for high supersonic Mach numbers and heated jets.

3.   Examination of a simplified (two-dimensional, three-layer) model indicates that high temperatures in the jet can materially reduce the probability of encountering spikes. This is associated with the decrease in local Mach number for given jet velocity and increased speed of sound.

4.   Investigation of simplified models also suggests that the unexpected features are quasi-resonant effects (where the dominant part of a denominator passes through zero), and that spikes appear only for non-uniform velocity profiles.

5.   Integration over source position, velocity and frequency
(which occurs automatically in experimental observations) should
smooth these peaks. However the "spikes", because they may appear
and disappear within a one-degree (or less) angular range in the
far field, present computational difficulties.

6.   The "spikes" are apparently associated with very high ob-
served frequencies, and at present it may be necessary to ignore
this high frequency range in order to avoid computing problems in
some examples.

7.   Although some of the results of Part 1 are both unexpected
and imperfectly understood they cannot safely be ignored. Further
study is necessary to show their true significance.

Part 2   NEAR-FIELD DISTURBANCES FROM TRANSIENT SOURCES IN SUBSONIC JETS

Introduction

Two factors make the near-field investigation much more difficult than the study of the far field. First, it is not possible to choose a critical (or dominant) K for each point in the near field. The attempt to do so leads to non-localized and hence unrealistic near fields. The disturbance produced by any one source should tend to decrease as the observation point is moved away from the source (upstream or downstream), and this decrease does not appear for a single K. The second factor is that transient sources which pass through many cycles (a simple case which avoids a frequency integration) cannot be used because they also lead to a non-localized near field. Instead the sources must be restricted to lifetimes of the order of one cycle and an integration over frequency is required. A new assumption must be made here, the length of time the source exists.

Another complication associated with the near field is that regions of exponential decay cannot be immediately discarded as in the far field. One of these regions (Region F , with true waves in the jet and exponential decay outside; see Fig. 18) may contain resonant points (singularities) which offer some difficulties in numerical calculations.

In the following analyses we consider several cases in order of their difficulty. First, the stationary pulsating source in a homogeneous fluid of infinite extent is studied. Next, we examine the harmonic source in a uniform jet and, finally, the sequence of transient sources in a uniform jet.

In general we look at mean-square radial displacement and mean energy flow. However the energy flow for the harmonic source in the jet is omitted because this involves a very tedious hand calculation. (Programming for machine computation seemed inadvisable at this time.) For the transient source space-time correlations are considered also. Numerical results for the transient source case are limited, primarily because

experienced programming assistance was not available to this project.

The Near Field of a Stationary Source in a Homogeneous Fluid of Infinite Extent

This solution is almost trivial, involving the well-known spherically symmetrical pulsating source. However we choose to discuss it in the cylindrical coordinates appropriate for a jet.

In spherical coordinates

$$\phi = \frac{2\pi A}{R} \sin\left[\omega'(R-ct)\right] \tag{35}$$

where ϕ is velocity potential, A is an arbitrary amplitude, R is spherical radius, ω = frequency, $\omega' = \omega/c$, c = speed of sound and t = time.

$$R = \sqrt{x^2+y^2+z^2} \tag{36}$$

where x, y, z are Cartesian coordinates, or

$$R = \sqrt{x^2+r^2} \tag{37}$$

where r is the cylindrical radius and x the axial direction.

In cylindrical coordinates

$$\phi = \frac{2\pi A}{\sqrt{x^2+r^2}} \sin\left[\omega'(\sqrt{x^2+r^2} - ct)\right] \tag{38}$$

To study instantaneous local energy flow, E , across the cylinder walls we need $\Delta p\, \phi_r$, where Δp is the perturbation pressure, $\Delta p = -\rho_0\, \phi_t$, with ρ_0 = mass density of the fluid.

$$E = - \rho_0 \, \phi_t \, \phi_r \qquad (39)$$

To study the radial displacement, η , we use

$$\eta = \int \phi_r \, dt \qquad (40)$$

The time mean of the energy flow, $\bar{E}$, is

$$\bar{E} = \frac{2\rho_0 \pi^2 A^2 \omega'^2 cr}{(x^2+r^2)^{3/2}} \qquad (41)$$

The time mean of the radial displacement squared, $\overline{\eta^2}$, is

$$\overline{\eta^2} = \frac{2\pi^2 A^2 r^2}{\omega^2} \left[\frac{\omega'^2}{(x^2+r^2)^2} + \frac{1}{(x^2+r^2)^3} \right] \qquad (42)$$

Let λ = wavelength = $2\pi/\omega'$, $\omega' = \omega/c$. Then

$$\overline{\left(\frac{\eta rc}{2A}\right)^2} = \frac{(\lambda/r)^2}{8(1 + \frac{x^2}{r^2})^2} \left[\left(\frac{2\pi}{\lambda/r}\right)^2 + \frac{1}{1 + \frac{x^2}{r^2}} \right] \qquad (43)$$

In Fig. (16) we normalize to unity at $x/r = 0$, and show how the mean-square radial displacement, Eq. (43), falls off for points "upstream" or "downstream" on the fictitious cylinder walls. This is done for $\lambda/r \rightarrow \infty$ and for $\lambda/r \rightarrow 0$. Also we show from Eq. (41) how the normalized energy flow varies with x/r . The curves are symmetrical about $x/r = 0$.

These curves show source effects to be fairly well localized in this simple case, and can be used as a basis for comparison in later cases.
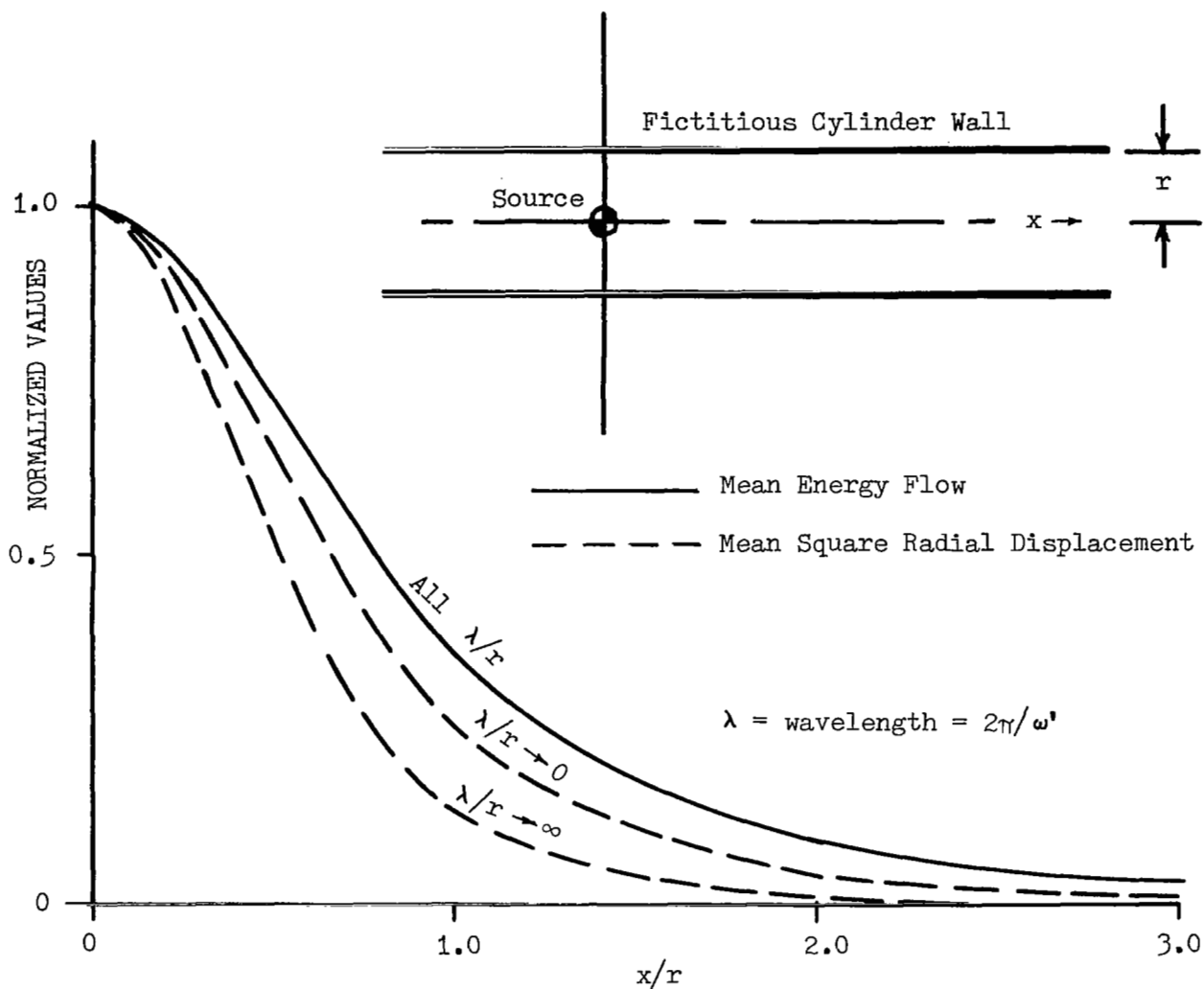
48

Fig. 16   SOURCE EFFECTS AT FICTITIOUS CYLINDER WALL FOR A
STATIONARY SOURCE IN A FLUID OF INFINITE EXTENT

The Near Field of a Permanent Pulsating Source at the Center of a Uniform Circular Jet

Introduction

Here we consider a permanent pulsating source (a harmonic source), on the centerline of a circular cylindrical jet. The jet velocity is uniform throughout, and the source drifts with the fluid perpetually. The origin of coordinates is fixed in the source, and we examine disturbances on the jet boundary upstream and downstream from the source. Mean-square radial displacements are compared with those for the previously studied stationary source in a homogeneous fluid of infinite extent (a zero-velocity jet case).

This problem requires fairly extensive calculations, but is still much simpler than the transient source problem treated later. Results are given for one example, obtained by hand-calculation using an HP-35 computer.

Development

The origin of coordinates is fixed in the source (see Fig. 17) with x the streamwise distance from the source and r the radial distance. In this coordinate system all the fluid within the jet is at rest and the acoustic equation is

$$\nabla^2 \phi = \frac{1}{c^2} \phi_{tt} \tag{44}$$

where ϕ is the velocity potential, ∇^2 is the Laplacian, c is the speed of sound and t is time.

The potential for a source at the origin is

$$\phi_s = \pi A \omega' \; \text{R.P.} \int_{-\infty}^{+\infty} e^{i\omega'(Kx-ct)} \; H_0^{(1)}(r\omega'\sqrt{1-K^2}) \, dK \tag{45}$$

where $A = $ (source strength)$/8\pi^2$, source strength being defined as
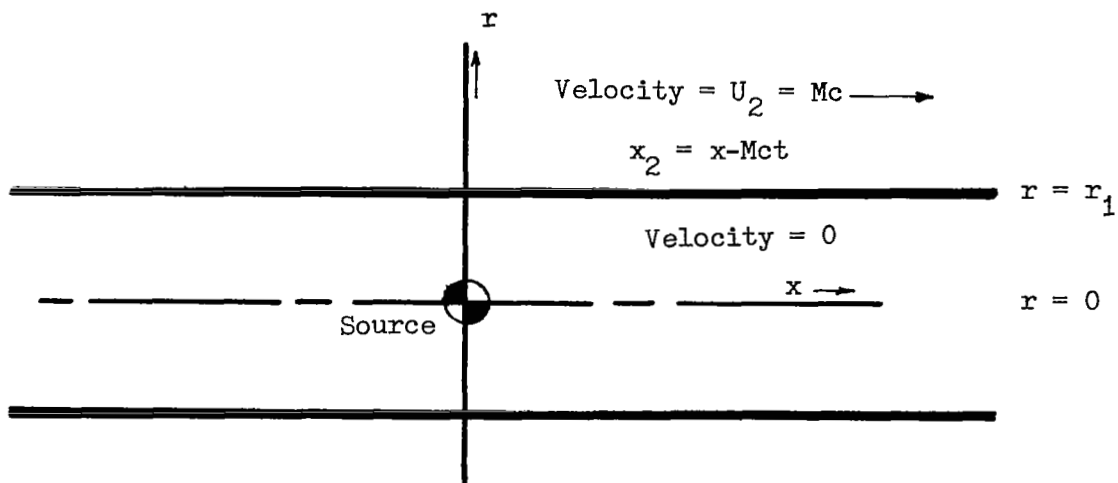
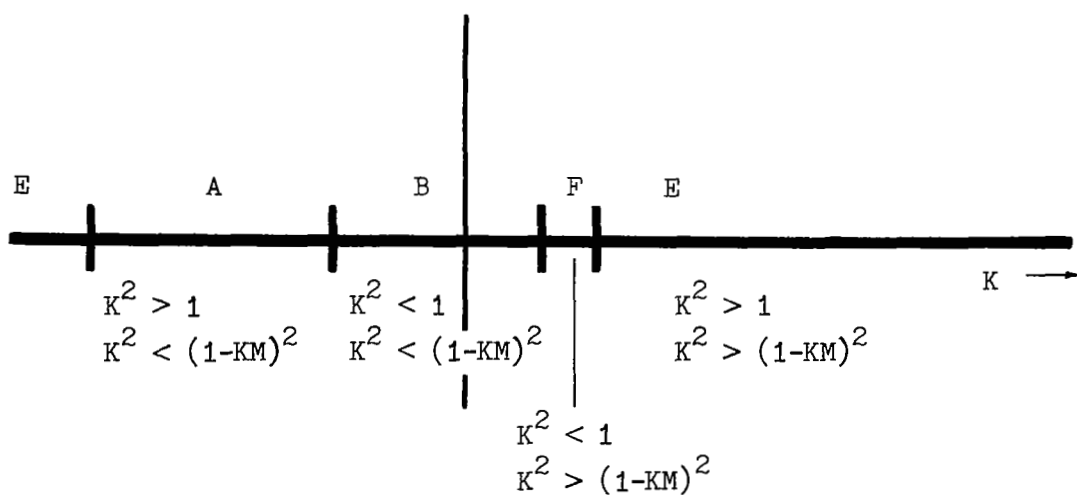Fig. 17   CIRCULAR CYLINDRICAL JET AND COORDINATE SYSTEM

Fig. 18   REGIONS OF THE K-LINE

maximum volume per unit time, ω is the source frequency, $\omega' = \omega/c$, k is wave number in the x-direction, $K = k/\omega'$, $H_0^{(1)}(\alpha)$ is the Hankel function of the first kind of order zero and argument α, and R.P. denotes "real part of".

Allowing for reflected waves the component potential $\phi(K)$ inside the jet is

$$\phi(K) = \dot{\pi}A\omega' \text{ R.P.}\left[e^{i\omega'(Kx-ct)}\left\{H_0^{(1)}(r\omega'\sqrt{1-K^2}) + \bar{R}\,J_0(r\omega'\sqrt{1-K^2})\right\}\right] \qquad (46)$$

where $\bar{R} = R'+iR''$, a complex reflection coefficient and J_0 is a zero order Bessel function.

Outside the jet the simple wave equation (Eq. (44)) must be satisfied for coordinates fixed in the ambient air, x_2 and r. The component potential, $\phi_2(K)$, allowing for outgoing waves only, is then

$$\phi_2(K) = \pi A\omega' \text{ R.P.}\left[\bar{S}\,e^{i\omega'[K(x_2+Mct)-ct]}H_0^{(1)}(r\omega'\sqrt{(1-KM)^2-K^2})\right] \qquad (47)$$

where $\bar{S} = S'+iS''$, and S' and S'' are in-phase and out-of-phase transmission coefficients.

The total potential outside the jet is

$$\phi_2 = \int_{-\infty}^{\infty} \phi_2(K)\,dK$$

To determine ϕ_2 we must find S' and S''. This is done by matching at the jet boundary the inside and outside values of pressure and of radial displacement. The pressure is $\Delta p = - \rho_0\,\phi_t$ inside and $\Delta p = - \rho_0\,\phi_{2_t}$ outside. The radial displacement is $\int \phi_r\,dt$ inside and $\int \phi_{2_r}\,dt$ outside, x being held constant in the former case and x_2 constant in the latter. We omit the details and record the result of applying the boundary conditions.

$$\phi_2 = \frac{2A}{r_1} \text{ R.P.} \int_{-\infty}^{\infty} \frac{i(KM-1) \, e^{i\omega'(Kx-ct)} \, H_0^{(1)}(r\omega'\sqrt{(1-KM)^2-K^2}) \, dK}{\left[(KM-1)^2 \sqrt{1-K^2} \, H_0^{(1)}[\ ] \, J_0'(\ ) - \sqrt{(1-KM)^2-K^2} \, H_0^{(1)'}[\ ] \, J_0(\ )\right]}$$

(48)

where

$$[\ ] = \left[r_1\omega'\sqrt{(1-KM)^2-K^2}\right]$$
$$(\ ) = (r_1\omega'\sqrt{1-K^2})$$

If we let $\eta = \int \phi_{2_r} \, dt$ with x_2 constant, then

$$\eta = \frac{2A}{r_1 c} \text{ R.P.} \int_{-\infty}^{\infty} \frac{\sqrt{(KM-1)^2-K^2} \, e^{i\omega'(Kx-ct)} \, H_0^{(1)'}(r\omega'\sqrt{(KM-1)^2-K^2}) \, dK}{\left[(KM-1)^2 \sqrt{1-K^2} \, H_0^{(1)}[\ ] \, J_0'(\ ) - \sqrt{(1-KM)^2-K^2} \, H_0^{(1)'}[\ ] \, J_0(\ )\right]}$$

(49)

The calculation of η from Eq. (49) is time consuming. First, the real part of the integrand must be found for four different K regions (see Fig. 18). Fairly extensive numerical computations must be made to obtain the integrand in each of the four regions, and then the numerical integration must be performed. For each value of x/r_1 investigated the integrand must be altered and a new integration performed. Since $\sin(\omega t)$ and $\cos(\omega t)$ terms can be removed from under the integral sign it is convenient to calculate $\overline{\eta^2}$, the time mean of η^2.

We do not include these tedious steps, but simply plot the final results for mean-square radial displacement at the edge of the jet versus streamwise position (see Fig. 19). In the example chosen the Mach number (M) is 0.5, the Strouhal number (S_T) is 0.2 and the ratio of wavelength to jet radius (λ/r_1) is 20.

Discussion

From Fig. 19 it is clear that the mean-square radial displacements at the jet edge fall off fairly rapidly with distance from the

$$\overline{\left(\frac{\eta r_1 c}{2A}\right)^2}$$

Mach No. = 0
(Stationary source
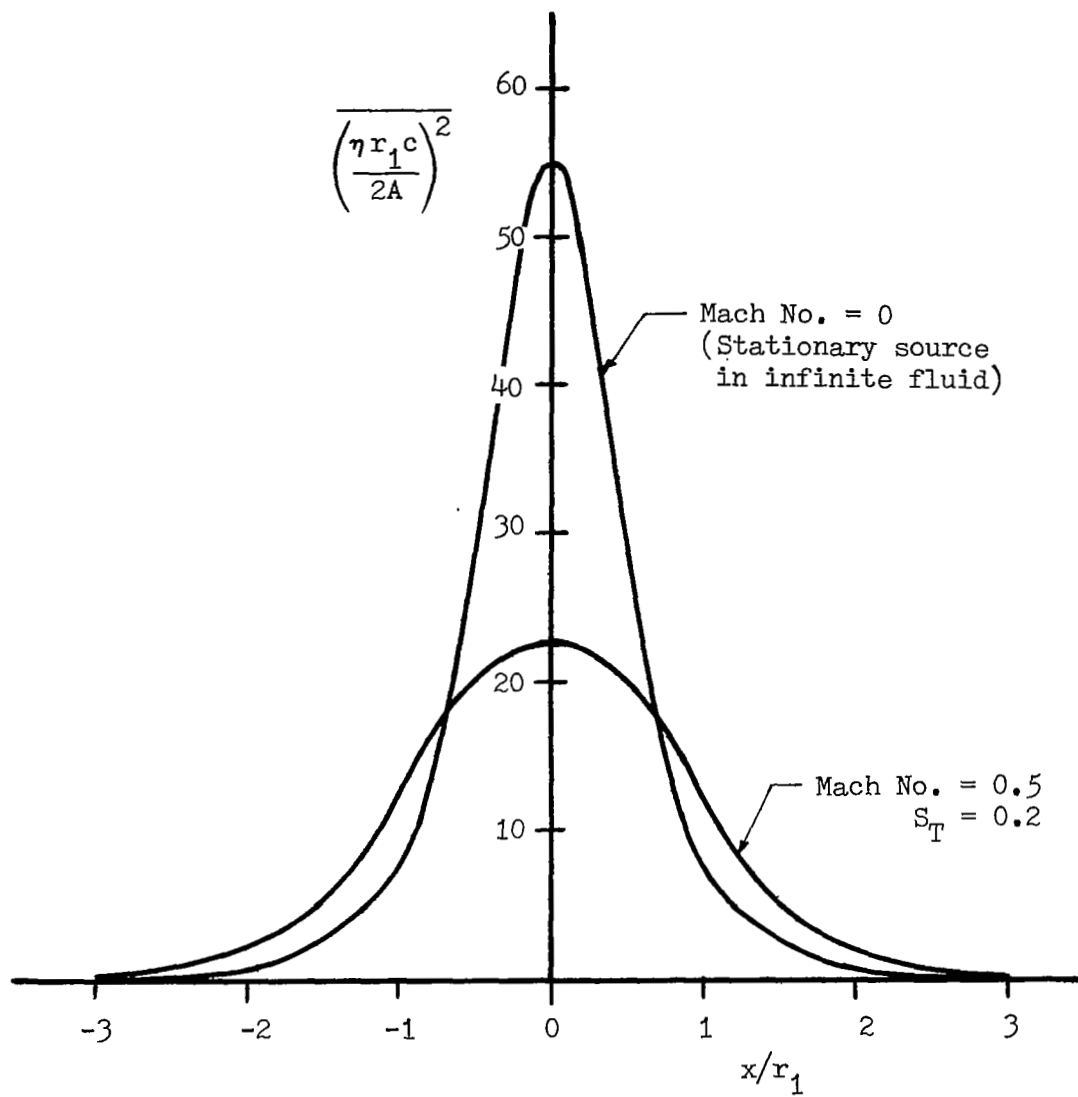in infinite fluid)

Mach No. = 0.5
S_T = 0.2

x/r_1

Fig. 19   COMPARISON OF MEAN-SQUARE RADIAL DISPLACEMENTS AT
JET EDGE FOR JET MACH NUMBERS OF ZERO AND 0.5
(HARMONIC SOURCES DRIFTING IN JET; λ/r_1 = 20)

54

source (upstream or downstream). However the rate of decrease is considerably less for M = 0.5 than for the stationary source (or zero velocity jet). One might speculate that reflections from the edge of the jet tend to prevent the source effects from leaving the jet cylinder.

It would be interesting to study the energy flow here, but this is a more difficult numerical problem and time does not permit. The energy flow should show greater asymmetry between the upstream and downstream directions. (An almost imperceptible asymmetry exists in Fig. 19 for the harmonic source in the jet.)

It would also be interesting to study a shear layer case to compare with the uniform velocity jet.

It must be remembered that the source in the jet is a continuously operating source (a harmonic source), not a transient source. The transient source (or sequence of transient sources) will be considered next. The coordinate system can then be fixed in the jet nozzle instead of traveling with the source.

The Near Field of a Sequence of Transient Sources at the Center of a Uniform Circular Jet

Mean-Square Radial Displacement

For a permanent (harmonic) source of generating frequency ω, let the radial displacement of a fluid particle in the ambient air be $\eta(\omega, t)$. Then for a transient source of frequency ω_0 existing from $t = -2\pi n/\omega_0$ to $t = +2\pi n/\omega_0$ (2n cycles):

$$\eta(\omega_0, t) = \frac{2\omega_0}{\pi} \int_0^\infty \frac{\eta(\omega, t) \sin(2\pi n\omega/\omega_0) \, d\omega}{(\omega^2 - \omega_0^2)} \tag{50}$$

This corresponds to the Fourier integral construction of a transient

55

process from all frequencies of a permanent one[13].

$\eta^2(\omega_0,t)$ can then be written as a double integral using Ω as a dummy variable for one integration:

$$\eta^2(\omega_0,t) = \frac{4\omega_0^2}{\pi^2} \int_0^\infty \int_0^\infty \frac{\eta(\omega,t) \sin(2\pi m\omega/\omega_0) \eta(\Omega,t) \sin(2\pi m\Omega/\omega_0) \, d\Omega \, d\omega}{(\omega^2-\omega_0^2)(\Omega^2-\omega_0^2)}$$

(51)

$\eta(\omega,t)$ and $\eta(\Omega,t)$ are given by Eq. (49) of the preceding section. (Ω and K' are substituted for ω and K in the second case.) For brevity we write them as

$$\eta(\omega,t) = \text{R.P.} \int_{-\infty}^\infty F(K,\omega,t) \, dK$$

$$\eta(\Omega,t) = \text{R.P.} \int_{-\infty}^\infty F(K',\Omega,t) \, dK'$$

(52)

Substituting Eq. (52) into Eq. (51) gives a quadruple integral for $\eta^2(\omega_0,t)$. To get the mean-square value of η , $\overline{\eta^2}$, for a sequence of transient sources we must integrate over a sufficiently large time (T) and divide by $4\pi m/\omega_0$, the time interval between the arrival (at a fixed point in the ambient air) of the initial impulse from one transient source and the initial impulse from the next transient source.

$$\overline{\eta^2}(\omega_0) = \frac{\omega_0^3}{\pi^3 n} \int_0^\infty \frac{\sin(2\pi m\omega/\omega_0)}{(\omega^2-\omega_0^2)} \int_0^\infty \frac{\sin(2\pi m\Omega/\omega_0)}{(\Omega^2-\omega_0^2)} \int_{-\infty}^\infty \int_{-\infty}^\infty \cdot$$

$$\cdot \int_{-\frac{T}{2}}^{\frac{T}{2}} F_R(K,\omega,t) F_R(K',\Omega,t) \, dt \, dK' \, dK \, d\Omega \, d\omega$$

(53)

where the integration in t is performed with x_2 constant. (Note that $x_2 = x - Mct$.)

It is now convenient to make the time dependence of F explicit so that the time integration can be performed.

$$F(K,\omega,t) = f(K,\omega) \, e^{i\omega t(KM-1)} \tag{54}$$

$f(K,\omega)$ is defined through reference to Eq. (49). $F(K',\Omega,t)$ and $f(K',\Omega)$ are obtained from $F(K,\omega,t)$ and $f(K,\omega)$ simply by substituting K' for K and Ω for ω .

$$f(K,\omega) = \frac{2A}{r_1 c} \frac{\sqrt{(1-KM)^2 - K^2} \, H_0^{(1)'}(r\omega'\sqrt{(1-KM)^2 - K^2}) \, e^{i\omega' K x_2}}{\left[(KM-1)^2 \sqrt{1-K^2} \, H_0^{(1)}[\ ] \, J_0'(\ ) - \sqrt{(1-KM)^2 - K^2} \, H_0^{(1)'}[\ ] \, J_0(\ )\right]} \tag{55}$$

$$\begin{aligned} [\ ] &= \left[r_1 \omega' \sqrt{(1-KM)^2 - K^2}\right] \\ (\ ) &= (r_1 \omega' \sqrt{1-K^2}) \end{aligned} \tag{56}$$

(Note that the argument of the Hankel function in the numerator contains r instead of r_1 .) Now, denoting $F = F_R + iF_I$, etc., we have

$$F_R(K,\omega,t) = f_R(K,\omega) \cos\left[\omega t(KM-1)\right] - f_I(K,\omega) \sin\left[\omega t(KM-1)\right]$$

and so

$$\begin{aligned} \overline{\eta^2}(\omega_0) = \frac{\omega_0^3}{\pi^3 n} \int_0^\infty \frac{\sin(2\pi n\omega/\omega_0)}{(\omega^2 - \omega_0^2)} \int_0^\infty \frac{\sin(2\pi n\Omega/\omega_0)}{(\Omega^2 - \omega_0^2)} \int_{-\infty}^\infty \int_{-\infty}^\infty \\ \cdot \left[f_R(K,\omega) \, f_R(K',\Omega) \int_{-T/2}^{T/2} \cos\left[\omega t(KM-1)\right] \cos\left[\Omega t(K'M-1)\right] dt \right. \\ \left. + f_I(K,\omega) \, f_I(K',\Omega) \int_{-T/2}^{T/2} \sin\left[\omega t(KM-1)\right] \sin\left[\Omega t(K'M-1)\right] dt \right] dK' \, dK \, d\Omega \, d\omega \end{aligned} \tag{57}$$

Here the integrals involving sin( ) cos( ) products have been omitted since the integrands are anti-symmetrical over the range $-T/2$ to $+T/2$ and contribute nothing.

The time integration is readily performed to give terms of the type

$$\frac{\sin\left\{\left[\omega(KM-1) - \Omega(K'M-1)\right]\frac{T}{2}\right\}}{\left[\omega(KM-1) - \Omega(K'M-1)\right]}$$

$$\frac{\sin\left\{\left[\omega(KM-1) + \Omega(K'M-1)\right]\frac{T}{2}\right\}}{\left[\omega(KM-1) + \Omega(K'M-1)\right]}$$

(58)

We next consider the integration in K' and for convenience let T become large. The integrands are then slowly varying functions of K' multiplied by functions of the above type which oscillate rapidly about zero as K' varies. Such functions interact weakly, and substantial contributions to the integral occur (a) when the rapidly varying function ceases to be rapidly varying (e.g. at stationary phase points), or (b) when the slowly varying function becomes rapidly varying (i.e. at singular points). This case is of the latter type, and so we investigate the singular points defined by

$$\omega(KM-1) \mp \Omega(K'M-1) = 0$$

or

$$K'_c = (\omega KM - \omega + \Omega)/\Omega M$$

and

(59)

$$K'_c = (-\omega KM + \omega + \Omega)/\Omega M$$

In the neighborhood of a singular point let $K' = K'_c + \delta$. Then integrating over this neighborhood produces integrals of the type

$$I = \int_{-\epsilon}^{\epsilon} \frac{\sin(\Omega M \frac{T}{2} \delta)\ d\delta}{\Omega M \delta} \tag{60}$$

which can be evaluated as $\pi/\Omega M$, remembering that $T \to \infty$. We then get

$$\overline{\eta^2}(\omega_0) = \frac{\omega_0^3}{\pi^2 n M} \int_0^\infty \frac{\sin(2\pi m \omega/\omega_0)}{(\omega^2 - \omega_0^2)} \int_0^\infty \frac{\sin(2\pi m \Omega/\omega_0)}{(\Omega^2 - \omega_0^2)^2} \int_{-\infty}^\infty \cdot$$

$$\cdot \frac{1}{\Omega} \left[f_R(K,\omega)\ f_R\left(\frac{\omega KM - \omega + \Omega}{\Omega M}, \Omega \right) \right.$$

$$+ f_I(K,\omega)\ f_I\left(\frac{\omega KM - \omega + \Omega}{\Omega M}, \Omega \right)$$

$$+ f_R(K,\omega)\ f_R\left(\frac{-\omega KM + \omega + \Omega}{\Omega M}, \Omega \right)$$

$$\left. - f_I(K,\omega)\ f_I\left(\frac{-\omega KM + \omega + \Omega}{\Omega M}, \Omega \right) \right]\ dK\ d\Omega\ d\omega \tag{61}$$

In Figs. 20 and 21 the preliminary results of calculations for $\overline{\eta^2}$ from Eq. (61) are presented. Fig. 20 shows a decrease in $\overline{\eta^2}$ with increasing distance radially outward from the jet. This would of course be expected. Fig. 21 shows that, for $r/r_1 = 1$ and $r/r_1 = 3$ most of the mean-square radial displacement ($\overline{\eta^2}$) is confined to the streamwise stations through which the transient source passes (a distance of ten jet diameters in this case).

For $r/r_1 = 1$ and $r/r_1 = 3$ there are large fluctuations in $\overline{\eta^2}$. It is not definitely known what causes this. These observation positions are very close to the source path in terms of the path length (20 r_1).

One might speculate that most of the contribution to $\overline{\eta^2}$ occurs when
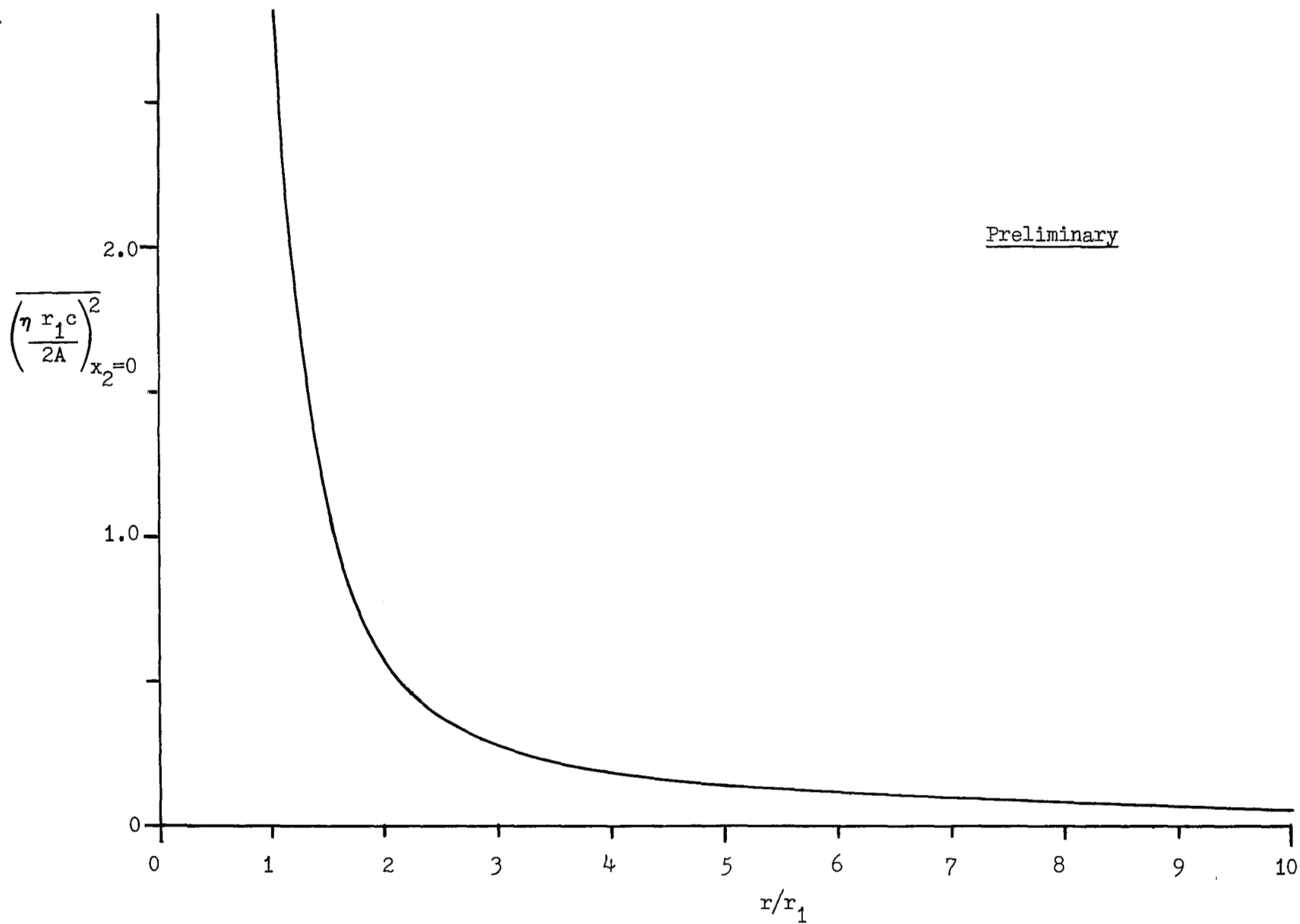
Fig. 20   VARIATION OF MEAN-SQUARE RADIAL DISPLACEMENT WITH RADIUS

Transient Source
$M = 0.5$, $S_T = 0.2$

$\dfrac{r}{r_1} = 1$

$\dfrac{r}{r_1} = 3$

$\dfrac{r}{r_1} = 10$

$\dfrac{\overline{\eta^2}}{(\overline{\eta^2})_{x_2=0}}$

Source   Path

$x_2/2r_1$

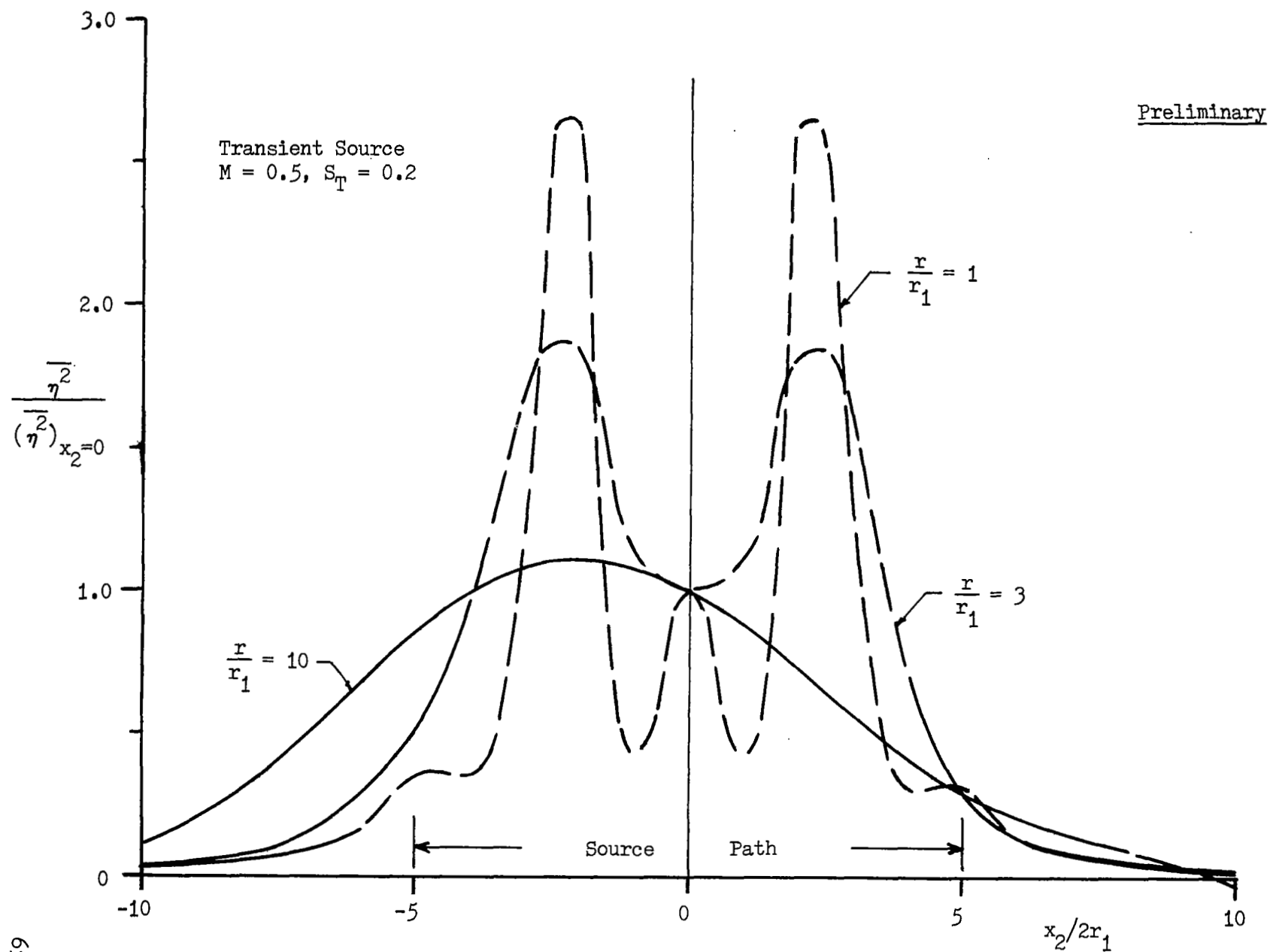-10   -5   0   5   10

61

Fig. 21   VARIATION OF MEAN-SQUARE RADIAL DISPLACEMENT WITH DISTANCE FROM SOURCE PATH

the source passes beneath the observation point. Since the phase of
the source has not yet been made random with respect to source position
on the path, some fluctuations in source effect with observation point
might possibly be attributed to this. These fluctuations seem to disap-
pear (or be greatly reduced) for $r/r_1 = 10$.

Fig. 21 also shows that the downstream disturbances exceed the up-
stream disturbances for $r/r_1 = 10$. Such a trend is very pronounced in
the far field, and it is quite interesting that it shows so clearly in
the near field (assuming these preliminary calculations to be sufficiently
accurate).

The rather large streamwise extent of substantial disturbances (ten
diameters) indicates the necessity for using transient sources of very
short lifetime to obtain realistic results in the near field. The source
of this example has a lifetime of two cycles. It might be desirable to
reduce this to one cycle or even one-half cycle (though some modifica-
tion of the equations is necessary).

Note that a similar problem arises in the more realistic expanding
jet. If such a model is to provide the correct far-field pressures the
sources should move with the jet fluid. Therefore the sources should
be transient and have very short effective lifetimes.

For either the cylindrical or the expanding jet it may be possible
that some simulation of convective effects can be achieved using sources
stationary with respect to the ambient air. Such sources are in motion
with respect to the immediately surrounding fluid (i.e. the jet) and
so are of many types[15]. Each type has a different relation between
downstream and upstream radiation. It is possible that _some_ type might
give usable pseudo-convective effects, but this is only a conjecture at
present, and thorough investigation would be required.

An alternative form of Eq. (61) which is possibly more convenient
is obtained by introducing the _observed_ frequency, ω^*, for an observer
at rest in the ambient air. (ω is the _generating_ frequency.)

$$\frac{\omega^*}{\omega} = (1 - KM_s) \tag{62}$$

where M_s is the source Mach number. Here the subscript s may be dropped since the jet has a uniform Mach number and the source travels with it. (Note that for $K = K_c = \cos\theta/(1+M_s\cos\theta)$, $\omega^* = \omega/(1+M_s\cos\theta)$, which checks the expression for ω^* previously used in the far field.)

From Eq. (62)

$$K = (\omega-\omega^*)/M\omega \qquad \text{and} \qquad dK = -d\omega^*/M\omega \qquad (63)$$

Eliminating K from Eq. (61) gives

$$\overline{\eta^2}(\omega_0) = \frac{\omega_0^3}{\pi^2 nM^2}\int_0^\infty \frac{\sin(2\pi m\omega/\omega_0)}{\omega(\omega^2-\omega_0^2)}\int_0^\infty \frac{\sin(2\pi n\Omega/\omega_0)}{\Omega(\Omega^2-\omega_0^2)}\int_{-\infty}^\infty \cdot$$

$$\cdot\left[f_R(\frac{\omega-\omega^*}{M\omega},\omega)\, f_R(\frac{\Omega-\omega^*}{M\Omega},\Omega) \right.$$

$$+ f_R(\frac{\omega-\omega^*}{M\omega},\omega)\, f_R(\frac{\Omega+\omega^*}{M\Omega},\Omega)$$

$$+ f_I(\frac{\omega-\omega^*}{M\omega},\omega)\, f_I(\frac{\Omega-\omega^*}{M\Omega},\Omega)$$

$$\left. - f_I(\frac{\omega-\omega^*}{M\omega},\omega)\, f_I(\frac{\Omega+\omega^*}{M\Omega},\Omega) \right]\, d\omega^*\, d\Omega\, d\omega \qquad (64)$$

A triple numerical integration is still required to obtain the mean-square radial displacement at any point outside the jet. However it is possible that the response in a narrow band of observed frequencies in the neighborhood of ω^* might be obtained by a double integration.

(Note that the $\overline{\eta^2}$ for $-\omega^*$ must be added to that for $+\omega^*$ in such cases.)

Mean Energy Flow

The rate of energy flow (E) across a unit area of a circular cylinder is the product of the perturbation pressure times the radial velocity, or

$$E = - \rho_0 \, \phi_{2_t} \, \phi_{2_r} \tag{65}$$

It is E and $\bar{E}$ which we want to find now instead of η^2 and $\overline{\eta^2}$. ($\eta = \int \phi_{2_r} \, dt$ with x_2 constant.)

Since the analysis proceeds almost exactly as before we merely note that instead of $f(K,\omega)$ and $f(K',\Omega)$ we now have $g_1(K,\omega)$, $g_2(K',\Omega)$, where

$$g_1(K,\omega) = \frac{2A\omega'}{r_1} \frac{i(KM-1) \sqrt{(1-KM)^2-K^2} \, H_0^{(1)}{}'(r\omega'\sqrt{(1-KM)^2-K^2}) \, e^{i\omega'Kx_2}}{\left[(KM-1)^2 \sqrt{1-K^2} \, H_0^{(1)}[\ ] \, J_0{}'(\ ) - \sqrt{(1-KM)^2-K^2} \, H_0^{(1)}{}'[\ ] \, J_0(\ ) \right]} \tag{66}$$

$$g_2(K',\Omega) = \frac{-2A\Omega \, (K'M-1)^2 \, H_0^{(1)}(r\Omega'\sqrt{(1-K'M)^2-K'^2}) \, e^{i\Omega'K'x_2}}{r_1 \left[(K'M-1)^2 \sqrt{1-K'^2} \, H_0^{(1)}[\ ] \, J_0{}'(\ ) - \sqrt{(1-K'M)^2-K'^2} \, H_0^{(1)}{}'[\ ] \, J_0(\ ) \right]} \tag{67}$$

(Note that $\Omega' = \Omega/c$ just as $\omega' = \omega/c$. $[\ ]$ and $(\ )$ in Eq. (66) are defined in Eq. (56). The same definitions apply in Eq. (67) if K' is substituted for K and Ω' for ω'.)

$$\overline{E}(\omega_0) = -\frac{\rho_0 \omega_0^3}{\pi^2 nM^2} \int_0^\infty \frac{\sin(2\pi n\omega/\omega_0)}{\omega(\omega^2-\omega_0^2)} \int_0^\infty \frac{\sin(2\pi n\Omega/\omega_0)}{\Omega(\Omega^2-\omega_0^2)} \int_{-\infty}^\infty \cdot$$

$$\cdot \left[g_{1_R}\left(\frac{\omega-\omega^*}{M\omega} , \omega \right) g_{2_R}\left(\frac{\Omega-\omega^*}{M\Omega} , \Omega \right) \right.$$

$$+ g_{1_R}\left(\frac{\omega-\omega^*}{M\omega} , \omega \right) g_{2_R}\left(\frac{\Omega+\omega^*}{M\Omega} , \Omega \right)$$

$$+ g_{1_I}\left(\frac{\omega-\omega^*}{M\omega} , \omega \right) g_{2_I}\left(\frac{\Omega-\omega^*}{M\Omega} , \Omega \right)$$

$$\left. - g_{1_I}\left(\frac{\omega-\omega^*}{M\omega} , \omega \right) g_{2_I}\left(\frac{\Omega+\omega^*}{M\Omega} , \Omega \right) \right] d\omega^* \, d\Omega \, d\omega$$

$$(68)$$

$\overline{E}(\omega_0)$ is the time mean of the energy flow across the cylinder wall per unit area and per unit time. ω_0 is the frequency for each transient source, which exists for just $2n$ cycles. Formally n should be an integer, but actually correct answers are obtained for one cycle when $n = 1/2$. ω^* is the frequency recorded by an observer at rest in the ambient air.

Space-Time Correlations in the Near Field

Introduction

One part of this work was directed towards the determination of space-time correlations of the pressure gradient in the near field for comparison with in-house research at Langley Research Center.

The mathematical formulation of this is not basically more diffi-cult than the treatment of energy flow just considered. However two problems arise. First, the introduction of pressure gradients (higher

derivatives) gives rise to a convergence problem. This can be handled without much difficulty. Second, the introduction of two new parameters, a space interval and a time interval, tends to greatly increase the volume of data to be obtained.

Again we consider first the simple case of a pulsating source at rest in a homogeneous fluid. Then transient sources at rest in a homogeneous fluid are investigated. Finally, the sequence of transient sources at the center of a uniform-velocity circular jet is studied.

The Stationary Source in a Homogeneous Fluid

The velocity potential for this source in cylindrical coordinates (see Eq. (38)) is

$$\phi = \frac{2\pi A}{\sqrt{x^2+r^2}} \ \sin\left[\omega'(\sqrt{x^2+r^2} - ct)\right] \tag{69}$$

The pressure gradient in the radial (r) direction is $\Delta p_r = - \rho_0 \, \phi_{tr}$ and if we retain only the portion associated with true sound Δp_r is

$$\Delta p_r(x,t) = - \frac{2\pi A \rho_0 \omega \omega' r}{x^2+r^2} \ \sin\left[\omega'(\sqrt{x^2+r^2} - ct)\right] \tag{70}$$

If we let ξ be a space interval in the axial (x) direction, and τ a time interval, then

$$\Delta p_r(x+\xi, t+\tau) = - \frac{2\pi A \rho_0 \omega \omega' r}{\left[(x+\xi)^2+r^2\right]} \ \sin\left[\omega'(\sqrt{(x+\xi)^2+r^2} - c(t+\tau))\right] \tag{71}$$

The correlation function is

$$\text{corr. fn.} = \lim_{T \to \infty} \frac{1}{T} \int_{-T/2}^{+T/2} \Delta p_r(x+\xi, t+\tau) \, \Delta p_r(x,t) \, dt \tag{72}$$

66

and using the two preceding equations we get

$$\text{corr. fn.} = \frac{2\pi^2 A^2 \rho_0{}^2 \omega^2 \omega'^2 r^2}{\left[(x+\xi)^2+r^2\right]\left[x^2+r^2\right]} \cos\left[\omega'\sqrt{(x+\xi)^2+r^2} - \omega'\sqrt{x^2+r^2} - \omega\tau\right] \qquad (73)$$

This correlation function does not die out with increasing time interval (τ), and so is unrealistic for the turbulent jet problem. We next examine the transient source which is more realistic.

If we assume that the transient source behavior is represented by a portion of a sine wave (see Fig. 22a, where n is set equal to 1) the radial pressure gradient Δp_r is (using Fourier integral representation as in Eq. (50))

$$\Delta p_r(x,t) = \frac{2\omega_0}{\pi} \frac{(-2\pi A\rho_0)r}{(x^2+r^2)c} \int_0^\infty \frac{\omega^2 \sin\left[\omega'(\sqrt{x^2+r^2} - ct)\right] \sin(2\pi n\omega/\omega_0)\, d\omega}{(\omega^2-\omega_0{}^2)}$$

$$(74)$$

At large ω the integrand contains only periodic functions (note ω^2 in numerator and denominator) and appears to present convergence problems. To avoid this we choose a smoother function (see Fig. 22b). Since this function ($\cos^2(\omega_0 t)$ between $-\pi/2\omega_0$ and $+\pi/2\omega_0$, and zero elsewhere) is symmetrical about $t = 0$ instead of anti-symmetrical, a cosine instead of sine is needed in the basic source potential. In cylindrical coordinates this is

$$\phi = \frac{2\pi A}{\sqrt{x^2+r^2}} \cos\left[\omega'(\sqrt{x^2+r^2} - ct)\right] \qquad (75)$$

The Fourier integral representation of the radial pressure gradient now becomes (for the true sound)

$$\Delta p_r(x,t) = \frac{4\omega_0{}^2(-2\pi A\rho_0)r}{\pi(x^2+r^2)c} \int_0^\infty \frac{\omega \cos\left[\omega'(\sqrt{x^2+r^2} - ct)\right] \sin(\pi\omega/2\omega_0)\, d\omega}{(4\omega_0{}^2-\omega^2)} \qquad (76)$$
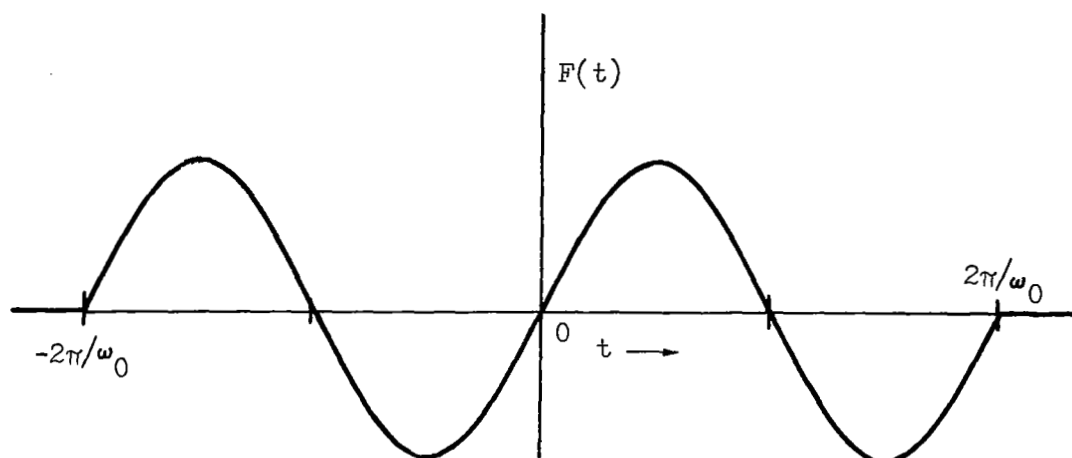
a)   (n = 1 for illustration)
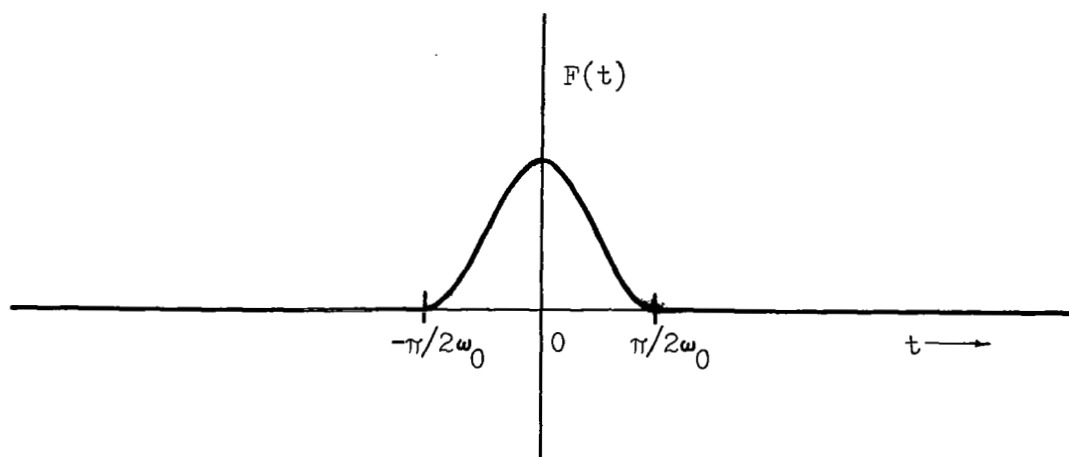
b)

Fig. 22   TRANSIENT SOURCE TIME HISTORIES

a) $F(t) = \sin(\omega_0 t)$ for $t^2 < (2\pi/\omega_0)^2$; $F(t) = 0$ elsewhere

b) $F(t) = \cos^2(\omega_0 t)$ for $t^2 < (\pi/2\omega_0)^2$; $F(t) = 0$ elsewhere

Smoothing the ends of the source time history produces ω/ω^2 in the integrand for large ω and improves the convergence.

For a sequence of transient sources the correlation function is

$$\text{corr. fn.} = \lim_{T\to\infty} \frac{\omega_0}{\pi} \int_{-\frac{T}{2}}^{\frac{T}{2}} \Delta p_r(x+\xi,t+\tau)\, \Delta p_r(x,t)\, dt \tag{77}$$

where π/ω_0 is the time interval between the arrival at a fixed point of the initial impulse from one transient source and the arrival of the initial impulse from the next transient source.

$$\text{corr. fn.} = \lim_{T\to\infty} \frac{16\omega_0^5(4A^2\rho_0^2 r^2)}{c^2(x^2+r^2)\left[(x+\xi)^2+r^2\right]} \int_0^\infty \int_0^\infty \int_{-\frac{T}{2}}^{\frac{T}{2}} \frac{\omega\Omega\,\sin(\pi\omega/2\omega_0)\,\sin(\pi\Omega/2\omega_0)}{(4\omega_0^2-\omega^2)(4\omega_0^2-\Omega^2)} \cdot$$

$$\cdot\, \cos\left[\omega'(\sqrt{x^2+r^2}-ct)\right]\cos\left[\Omega'(\sqrt{(x+\xi)^2+r^2}-c|t+\tau|)\right]\, dt\, d\Omega\, d\omega \tag{78}$$

The time integration can be made immediately. As $T\to\infty$ the Ω integration involves a function oscillating rapidly about zero, and the integral is evaluated from contributions near the singular point $\Omega=\omega$. The result is

$$\text{corr. fn.} = \frac{16\omega_0^4(4A^2\rho_0^2 r^2)}{c^2(x^2+r^2)\left[(x+\xi)^2+r^2\right]} \int_0^\infty \frac{(\omega/\omega_0)^2\,\sin^2(\pi\omega/2\omega_0)\,\cos(\omega\gamma/\omega_0)\,d(\omega/\omega_0)}{\left[(\omega/\omega_0)^2-4\right]^2} \tag{79}$$

where

$$\gamma = \frac{\omega_0}{c}\left[\sqrt{(x+\xi)^2+r^2} - \sqrt{x^2+r^2} - c\tau\right] \tag{80}$$

The integral can be evaluated (see Gradshteyn and Ryshik, Ref. 17,

#3.728, 7., p. 410, and let their $c = b + \epsilon$, $\epsilon \to 0$). For $0 < \gamma < \pi$ we get

$$\text{corr. fn.} = \frac{-4\pi A^2 \rho_0{}^2 \omega_0{}^4 r^2}{c^2(x^2+r^2)\left[(x+\xi)^2+r^2\right]} \left[\sin(2\gamma) + 2(\gamma-\pi)\cos(2\gamma)\right] \qquad (81)$$

For $\gamma > \pi$ the correlation function is identically zero, and the correlation function is symmetrical about $\gamma = 0$. Fig. 23 (from Eq. (81)) shows the effect of γ on the correlation function.

A transient source at rest in a homogeneous fluid produces disturbances which are confined completely to an expanding spherical shell. The thickness of the shell is c times the lifetime of the source. If the time interval, τ , is zero the space interval, ξ , can be chosen so that two points separated by a distance ξ in the x-direction are never in the expanding shell at the same time. The correlation is then identically zero. Similar situations can arise of course when τ is not zero.

It must be remembered that in a sequence of transient sources the phase of any one source is assumed random relative to the other sources. The correlation function is then not affected by interactions between pairs of sources.

Pressure Gradient Correlation Functions for a Sequence of Transient Sources at the Center of a Uniform Circular Jet

In order to avoid convergence problems, we adopt a smoothed time history for the transient sources (see Fig. 22b). Since this is symmetrical (instead of anti-symmetrical) about $t = 0$ it is necessary to modify the source potential ϕ_2 by taking the imaginary rather than the real part of the complex potential (see Eq. (48)). ϕ_2 is then

$$\text{corr. fn.} \cdot \left\{ \frac{c^2(x^2+r^2)\left[(x+\xi)^2+r^2\right]}{-4\pi A^2 \rho_0^2 \omega_0^4 r^2} \right\} \cdot$$
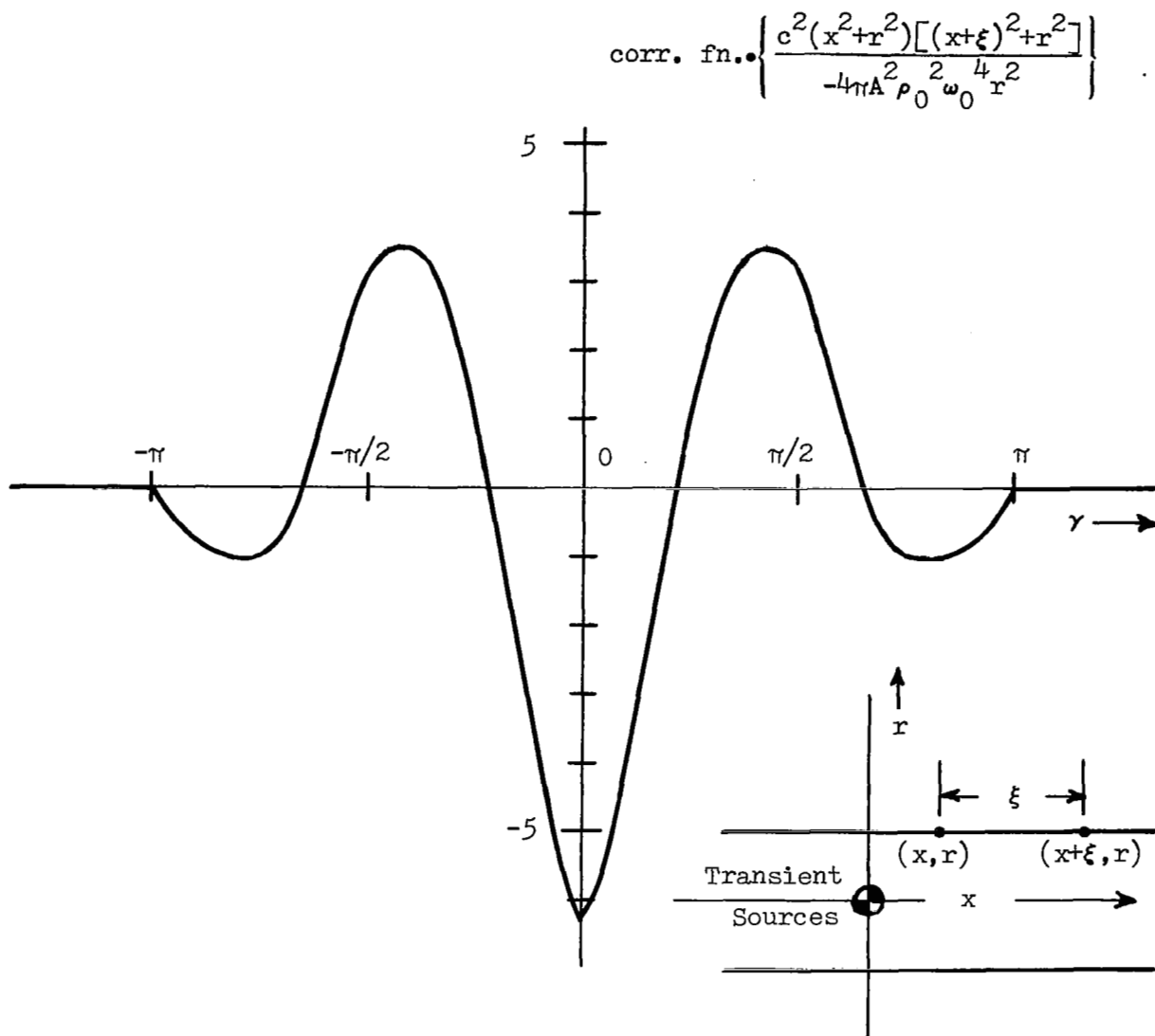
Fig. 23   PRESSURE GRADIENT CORRELATION FUNCTION vs γ FOR TRANSIENT
SOURCES AT REST IN A FLUID OF INFINITE EXTENT

(γ is a function of ξ and τ, the space and time intervals.
See Eqs. (80) and (81).)

$$\phi_2 = \frac{2A}{r_1} \text{I.P.} \int_{-\infty}^{\infty} \frac{i (KM-1) H_0^{(1)}(r\omega'\sqrt{2}) \, e^{i\omega'Kx_2} \, e^{i\omega t(KM-1)} \, dK}{\left[(KM-1)^2 \sqrt{1-K^2} H_0^{(1)}[\ ] J_0'(\ ) - \sqrt{2} H_0^{(1)'}[\ ] J_0(\ )\right]} \tag{82}$$

$$
\begin{aligned}
[\ ] &= \left[r_1\omega'\sqrt{2}\right] \\
(\ ) &= (r_1\omega'\sqrt{1-K^2} \\
\sqrt{2} &= \sqrt{(KM-1)^2-K^2}
\end{aligned}
\tag{83}
$$

The radial pressure gradient is $-\rho_0 \phi_{2_{rt}}$

$$\phi_{2_{rt}}(\omega,t) = \frac{-2A\omega'\omega}{r_1} \text{I.P.} \int_{-\infty}^{\infty} \frac{(KM-1)^2 \sqrt{2} H_0^{(1)'}(r\omega'\sqrt{2}) \, e^{i\omega'Kx_2} \, e^{i\omega t(KM-1)} \, dK}{\left[(KM-1)^2 \sqrt{1-K^2} H_0^{(1)}[\ ] J_0'(\ ) - \sqrt{2} H_0^{(1)'}[\ ] J_0(\ )\right]} \tag{84}$$

For the transient source we need $\phi_{2_{rt}}(\omega_0,t)$. The Fourier integral representation of this is

$$\phi_{2_{rt}}(\omega_0,t) = \frac{4\omega_0^2}{\pi} \int_0^{\infty} \frac{\phi_{2_{rt}}(\omega,t) \, \sin(\pi\omega/2\omega_0) \, d\omega}{\omega(4\omega_0^2-\omega^2)} \tag{85}$$

To simplify this expression let

$$
\begin{aligned}
\phi_{2_{rt}}(\omega,t,x_2) &= \text{I.P.} \int_{-\infty}^{\infty} G(K,\omega,t,x_2) \, dK \\
\phi_{2_{rt}}(\Omega,t+\tau,x_2+\xi) &= \text{I.P.} \int_{-\infty}^{\infty} G(K',\Omega,t+\tau,x_2+\xi) \, dK'
\end{aligned}
\tag{86}
$$

The space-time correlation function for the two points (x_2,r), $(x_2+\xi,r)$ is

$$\text{corr. fn.} = \lim_{T\to\infty} \frac{\omega_0}{\pi} \int_{-\frac{T}{2}}^{\frac{T}{2}} \Delta p_{rt}(\Omega, t+\tau, x_2+\xi)\, \Delta p_{rt}(\omega, t, x_2)\, dt \tag{87}$$

$$\text{corr. fn.} = \frac{16\rho_0^2\omega_0^2}{\pi^3} \int_0^\infty \frac{\sin(\pi\omega/2\omega_0)}{\omega(4\omega_0^2-\omega^2)} \int_0^\infty \frac{\sin(\pi\Omega/2\omega_0)}{\Omega(4\omega_0^2-\Omega^2)} \int_{-\infty}^\infty \int_{-\infty}^\infty \,\cdot$$

$$\cdot \int_{-\frac{T}{2}}^{\frac{T}{2}} G_I(K', \Omega, t+\tau, x_2+\xi)\, G_I(K, \omega, t, x_2)\, dt\, dK'\, dK\, d\Omega\, d\omega \tag{88}$$

In order to perform the time integration the term containing t is factored out, giving

$$G(K,\omega,t,x_2) = g(K,\omega,x_2)\, e^{i\omega t(KM-1)} \tag{89}$$

$$G(K',\Omega,t+\tau,x_2+\xi) = g(K',\Omega,x_2)\, e^{i\Omega t(K'M-1)}\ e^{i\Omega\left[\tau(K'M-1)+K'\xi/c\right]}$$

The imaginary parts of G required in the integrand are then

$$G_I(K,\omega,t,x_2) = g_I(K,\omega,x_2)\, \cos\left[\omega t(KM-1)\right] + g_R(K,\omega,x_2)\, \sin\left[\omega t(KM-1)\right] \tag{90}$$

$$
\begin{aligned}
G_I(K',\Omega,t+\tau,x_2+\xi) = {} & g_I(K',\Omega,x_2)\, \cos\left[\Omega t(K'M-1)\right]\, \cos\left[\Omega(\tau K'M-\tau+K'\xi/c)\right] \\
& - g_I(K',\Omega,x_2)\, \sin\left[\Omega t(K'M-1)\right]\, \sin\left[\Omega(\tau K'M-\tau+K'\xi/c)\right] \\
& + g_R(K',\Omega,x_2)\, \sin\left[\Omega t(K'M-1)\right]\, \cos\left[\Omega(\tau K'M-\tau+K'\xi/c)\right] \\
& + g_R(K',\Omega,x_2)\, \cos\left[\Omega t(K'M-1)\right]\, \sin\left[\Omega(\tau K'M-\tau+K'\xi/c)\right]
\end{aligned}
$$

In the integration range from $-T/2$ to $+T/2$ the anti-symmetric parts of the integrand can be omitted. Then

$$
\int_{-\frac{T}{2}}^{\frac{T}{2}} G_I(K',\Omega,t+\tau,x_2+\xi)\, G_I(K,\omega,t,x_2)\, dt =
$$

$$
\left(g_I(K,\omega,x_2) \left\{ g_I(K',\Omega,x_2) \cos\left[\Omega(\tau K'M-\tau+K'\xi/c)\right] \right. \right.
$$

$$
\left. \left. + g_R(K',\Omega,x_2) \sin\left[\Omega(\tau K'M-\tau+K'\xi/c)\right] \right\} \right) \cdot
$$

$$
\cdot \int_{-\frac{T}{2}}^{\frac{T}{2}} \cos\left[\omega t(KM-1)\right] \cos\left[\Omega t(K'M-1)\right]\, dt
$$

$$
+ \left(g_R(K,\omega,x_2) \left\{ g_R(K',\Omega,x_2) \cos\left[\Omega(\tau K'M-\tau+K'\xi/c)\right] \right. \right.
$$

$$
\left. \left. - g_I(K',\Omega,x_2) \sin\left[\Omega(\tau K'M-\tau+K'\xi/c)\right] \right\} \right) \cdot
$$

$$
\cdot \int_{-\frac{T}{2}}^{\frac{T}{2}} \sin\left[\omega t(KM-1)\right] \sin\left[\Omega t(K'M-1)\right]\, dt \tag{91}
$$

The time integration is simple and for $T \to \infty$ the integration in K' is obtained (as previously discussed) from the neighborhood of the singular points. A triple integral (in K,Ω,ω) remains to be determined in the expression for the correlation function. As before, we choose to rewrite this in terms of observed frequency, ω^*, noting that $K = (\omega-\omega^*)/M\omega$.

$$\text{corr. fn.} = \frac{16\rho_0{}^2\omega_0{}^5}{\pi^2 M^2} \int\limits_0^\infty \frac{\sin(\pi\omega/2\omega_0)}{\omega^2(4\omega_0{}^2-\omega^2)} \int\limits_0^\infty \frac{\sin(\pi\Omega/2\omega_0)}{\Omega^2(4\omega_0{}^2-\Omega^2)} \int\limits_{-\infty}^\infty \cdot$$

$$\cdot \left\{ g_I\left(\frac{\omega-\omega^*}{M\omega},\omega\right) \left[g_I\left(\frac{\Omega-\omega^*}{M\Omega},\Omega\right)\cos\gamma_1 + g_I\left(\frac{\Omega+\omega^*}{M\Omega},\Omega\right)\cos\gamma_2 \right. \right.$$

$$\left. + g_R\left(\frac{\Omega-\omega^*}{M\Omega},\Omega\right)\sin\gamma_1 + g_R\left(\frac{\Omega+\omega^*}{M\Omega},\Omega\right)\sin\gamma_2 \right]$$

$$+ g_R\left(\frac{\omega-\omega^*}{M\omega},\omega\right) \left[g_R\left(\frac{\Omega-\omega^*}{M\Omega},\Omega\right)\cos\gamma_1 - g_R\left(\frac{\Omega+\omega^*}{M\Omega},\Omega\right)\cos\gamma_2 \right.$$

$$\left. \left. - g_I\left(\frac{\Omega-\omega^*}{M\Omega},\Omega\right)\sin\gamma_1 + g_I\left(\frac{\Omega+\omega^*}{M\Omega},\Omega\right)\sin\gamma_2 \right] \right\} d\omega^* \, d\Omega \, d\omega$$

$$(92)$$

where

$$g(K,\omega) = \frac{-2A\omega'\omega\,(KM-1)^2\,\sqrt{2}\,H_0^{(1)'}(r\omega'\sqrt{2})\,e^{i\omega'Kx_2}}{r_1\left[(KM-1)^2\,\sqrt{1-K^2}\,H_0^{(1)}[\;]\,J_0{}'(\;) - \sqrt{2}\,H_0^{(1)'}[\;]\,J_0(\;)\right]}$$

$$(93)$$

$$\gamma_1 = (\Omega-\omega^*)(\xi/Mc) - \tau\omega^*$$

$$\gamma_2 = (\Omega+\omega^*)(\xi/Mc) + \tau\omega^*$$

$$\sqrt{2} = \frac{1}{M}\sqrt{(M^2-1)(\omega^{*2}/\omega^2) + 2(\omega^*/\omega) - 1}$$

$$\sqrt{1-K^2} = \frac{1}{M}\sqrt{(M^2-1) + 2(\omega^*/\omega) - (\omega^{*2}/\omega^2)}$$

$$KM-1 = -\omega^*/\omega$$

CONCLUSIONS - Part 2

1. A realistic picture of the near field must show disturbances dying out as the distance from a small region occupied by transient sources increases. The lifetime of each transient source must then be very brief (not merely finite), and this, plus the lack of a stationary phase approximation, requires integration over both frequency and wave number. These two integrations make near-field analysis much more difficult than far-field analysis.

2. A preliminary near-field analysis is made using coordinates fixed in a permanent pulsating source (a harmonic source). This source drifts with the fluid at the center of a uniform circular cylindrical jet. For a Mach number of 0.5 and a Strouhal number of 0.2 the streamwise extent of substantial disturbances is appreciably greater than for a Mach number of zero.

3. The near field is studied for a sequence of transient sources at the center of a uniform circular jet. Results here must be considered preliminary since a triple integration is performed numerically. The integration seems feasible, but the accuracy of the methods has not yet been completely explored. The preliminary results are reasonable. Most interesting is the appearance in the near field of the trend toward increased downstream disturbances which is so characteristic of the far field.

Appendix A

A TWO-DIMENSIONAL CHANNEL FLOW SHOWING RESONANT AND QUASI-RESONANT PEAKS

Introduction and Discussion

It is convenient to represent a pulsating source in a jet as the sum of components having all possible wavelengths in the streamwise direction. Some of these components are true waves, and some decay exponentially in the z-direction, normal to the flow. Each of these harmonic wave forms (infinitely long in the flow direction) moves at its own velocity relative to the source. The source itself moves with the local fluid, so the velocity of the waveform with respect to the fluid in any part of the idealized jet can be determined. Conversely, the velocity of the fluid relative to the waveform is known.

If we then approximate the fluid motion in some part of the jet by a uniform velocity flow it is tempting to study for the purpose of illustration a conventional channel flow where one side of the channel consists of a prescribed wavy wall. Some boundary condition must now be prescribed for the other wall of the channel. It is not possible to say precisely what this condition should be. However a generalized boundary condition of the form $a \, \phi_x(x, z_1) + b \, \phi_z(x+\gamma, z_1) = 0$ may be used. If $a = 0$ a flat rigid wall exists at $z = z_1$. If $b = 0$ a constant pressure surface exists at $z = z_1$. Other combinations of a, b and γ should correspond to the conditions existing in a jet though these combinations are not easily found.

The energy flow across the outer boundary of the channel is examined as a function of a non-dimensionalized wavelength in the flow direction. Various outer boundary conditions are considered. In some cases true resonant peaks appear (the entire denominator passing through zero). In other cases quasi-resonant peaks are evident (the dominant part of the denominator passing through zero). This highly simplified model therefore does show features resembling those appearing in the

complete shear layer jet, although the peaks appear in a plot of energy flow vs. wavelength rather than in mean-square pressure vs. far-field angle θ.

The above results are interesting and perhaps useful. However it must be emphasized that some very important features of the jet, such as the jet velocity relative to the ambient air and the velocity of the acoustical source, are concealed in the generalized boundary condition. This procedure could not readily be used for any quantitative prediction of the appearance of peaks in the idealized shear-layer jets which we are studying, but is possibly of value as a qualitative illustration.

Development

The development is here outlined very briefly since the problem is comparatively simple. Only supersonic flow is considered, this being the case of primary interest.

The origin of the x, z coordinate system is fixed in the mean plane of the channel's prescribed wavy wall (see Fig. 1A). The flow direction is x, the normal direction z. The flow obeys the equation

$$(M^2-1)\phi_{xx} - \phi_{zz} = 0 \tag{A-1}$$

where M is the undisturbed constant Mach number $(M > 1)$ and ϕ is the velocity potential. The prescribed wavy wall is at $z = 0$, the outer boundary of the channel is at $z = z_1$. Let

$$\phi_z = A \sin(k_1 x) \qquad \text{at} \quad z = 0 \tag{A-2}$$

and let

$$a \, \phi_x(x, z_1) + b \, \phi_z(x+\gamma, z_1) = 0 \qquad \text{at} \quad z = z_1 \tag{A-3}$$

where A prescribes the amplitude and k_1 the wave number of the wavy

78

The diagram shows:

$$a\,\phi_x(x,z_1) + b\,\phi_z(x+\gamma,z_1) = 0$$

Outer Boundary — $z = z_1$

$$(M^2-1)\phi_{xx} - \phi_{zz} = 0$$

$M > 1$

z

x

$z = 0$

Prescribed Wavy Wall

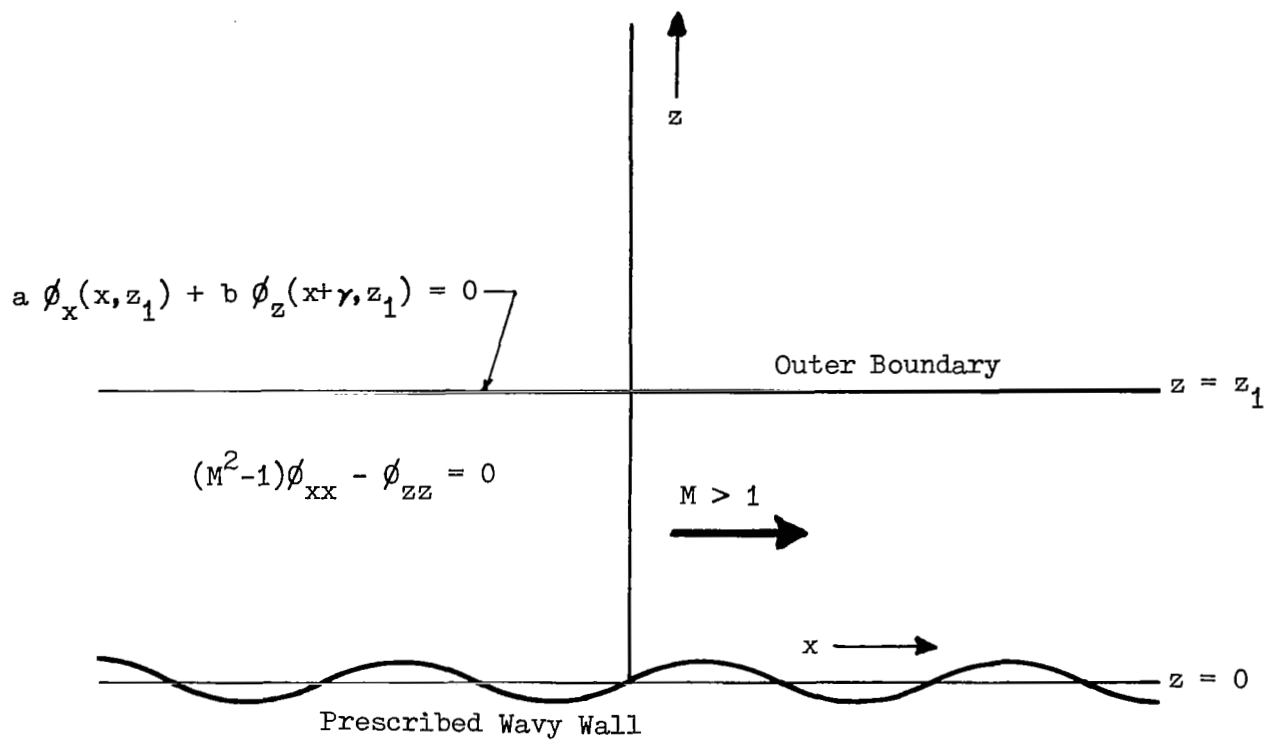Fig. 1A   THE TWO-DIMENSIONAL CHANNEL

wall, a and b are arbitrary constants and γ permits an arbitrary phase displacement between ϕ_x and ϕ_z at $z = z_1$.

The following expression for ϕ satisfies the partial differential equation (A-1) and the boundary conditions (A-2) and (A-3):

$$\phi = \frac{A}{k_2 \{\ \}} \left(\{\ \} \sin(k_1 x) \sin(k_2 z) + [\ ]_3 \sin(k_1 x) \cos(k_2 z) \right. $$
$$\left. + \frac{abk_1}{k_2} \cos(k_1 \gamma) \cos(k_1 x) \cos(k_2 z) \right) \qquad (A\text{-}4)$$

where

$$k_2^{\ 2} = k_1^{\ 2}(M^2 - 1)$$

$$\{\ \} = \{[\ ]_1^{\ 2} + b^2 \cos^2(k_1 \gamma) \sin^2(k_2 z_1)\}$$

$$[\ ]_1 = [(ak_1/k_2) \cos(k_2 z_1) - b \sin(k_1 \gamma) \sin(k_2 z_1)]_1 \qquad (A\text{-}5)$$

$$[\ ]_3 = [\tfrac{1}{2}(b^2 - a^2 \frac{k_1^{\ 2}}{k_2^{\ 2}}) \sin(2k_2 z_1) - \frac{abk_1}{k_2} \sin(k_1 \gamma) \cos(2k_2 z_1)]_3$$

It is convenient to examine the energy flow (relative to coordinates fixed in the fluid). This is independent of z and is given by $(-\rho M c\, \phi_x \phi_z)$, ρ being the mass density of the fluid and c the speed of sound. This is the local value, and any convenient z (e.g. $z = 0$) may be used. If we define by $\overline{E}$ the _mean_ energy flow per unit area, then

$$\overline{E} = \frac{A^2 ab\ k_1^{\ 2} \cos(k_1 \gamma)\ \rho M c}{2\ k_2^{\ 2}\ \{\ \}} \qquad (A\text{-}6)$$

where $\{\ \}$ is defined in Eq. (A-5) and b may be set equal to unity

without loss of generality.

For a specific example let $M = \sqrt{2}$ and $(k_1 \gamma) = 0$. Then $k_2{}^2 = k_1{}^2$ and

$$E^* = \frac{2\bar{E}}{A^2 \rho Mc} = \frac{a}{a^2 \cos^2(k_1 z_1) + \sin^2(k_1 z_1)} \tag{A-7}$$

For $a = 1$ the flow pattern is precisely that which occurs for an infinite fluid flowing past a wavy wall, and $E^* = 1$. If a is large (e.g. $a = 10$) then $a^2 \cos^2(k_1 z_1)$ is generally the dominant term in the denominator, but passes through zero for $(k_1 z_1) = \frac{\pi}{2}, \frac{3\pi}{2}$, etc. Thus quasi-resonant peaks appear near these $(k_1 z_1)$ values. If a is small (e.g. $a = 0.1$) then $\sin^2(k_1 z_1)$ is generally dominant but quasi-resonant peaks appear near $(k_1 z_1) = 0, \pi, 2\pi$, etc.

As $a \rightarrow \infty$ the outer boundary of the channel approaches a constant pressure surface and true resonances at $(k_1 z_1) = \frac{\pi}{2}, \frac{3\pi}{2}$, etc., are approached. As $a \rightarrow 0$ the outer boundary becomes a plane rigid wall, and true resonances at $(k_1 z_1) = 0, \pi, 2\pi$, etc., are approached.

Appendix B

THE HEATED THREE-LAYER TWO-DIMENSIONAL JET

The problem considered is that sketched in Fig. 13, but the three layers shown now have different temperatures and densities. Outside the jet (Region ②), the ambient air has temperature T_a, corresponding density ρ_a, and speed of sound c_a. In the outer layer of the jet (Region ①) these quantities are T_1, ρ_1, c_1, and in the central high velocity layer (Region ⓪) they are T_0, ρ_0, c_0.

If the velocity of the jet in Region ① is U_1 and the velocity in Region ⓪ is U_0, then the corresponding Mach numbers indicated in Fig. 13 are defined with respect to _ambient_ temperature:

$$M_1 = U_1/c_a$$
$$M_0 = U_0/c_a \qquad (B-1)$$

Standard thermodynamic relationships give also

$$\frac{\rho_1}{\rho_a} = \frac{T_a}{T_1} = \frac{c_a^{\,2}}{c_1^{\,2}}$$

$$\frac{\rho_0}{\rho_a} = \frac{T_a}{T_0} = \frac{c_a^{\,2}}{c_0^{\,2}} \qquad (B-2)$$

We further define

$$\omega' = \omega/c_a$$

$$K_1 = k_1/\omega' \,, \quad K_2 = k_2/\omega' \qquad (B-3)$$

$$K = \sqrt{K_1^{\,2} + K_2^{\,2}}$$

If the analysis described earlier in the report is modified to allow for the different temperatures of the three layers, Eq. (11) becomes

$$|\bar{s}|^2 = \frac{4(T_a/T_1)^2}{(1-M_1K_1)^2[K^2-(c_a/c_1)^2]} \quad \frac{N^2}{D_1^2+{\mu_1'}^2D_2^2} \qquad \text{(B-4)}$$

where the previous definitions of N, D_1, D_2 given by Eq. (12) for the symmetric case and Eq. (14) for the anti-symmetric case retain their previous forms but the parameters therein defined by Eq. (13) for the unheated jet now become

$$\sigma' = \omega'(a_2-a_1)\sqrt{K^2-(c_a/c_1)^2}$$

$$\xi' = \omega'(z_s-a_1)\sqrt{K^2-(c_a/c_1)^2}$$

$$\mu_1' = \frac{(T_a/T_1)\sqrt{(1-K_1M_1)^2-K^2}}{(1-M_1K_1)^2\sqrt{K^2-(c_a/c_1)^2}}$$

$$\mu_2' = \frac{(T_0/T_1)\sqrt{(c_a/c_0)^2[1+K_1(M_0-M_1)]^2-K^2}}{[1+K_1(M_0-M_1)]^2\sqrt{K^2-(c_a/c_1)^2}}$$

$$\qquad \text{(B-5)}$$

and α, defined for the unheated jet in Eq. (8), becomes

$$\alpha = \omega'a_1\sqrt{(c_a/c_0)^2[1+K_1(M_0-M_1)]^2-K^2} \qquad \text{(B-6)}$$

Comparison indicates that the statements made for the unheated jet are still applicable. That is, for very large K, μ_1' is small. D_1^2 then is normally the dominant term of the denominator for large K, and spikes in the far-field pressure distribution will be found at the zeros of D_1. These occur for the symmetric case when

$$\tanh\sigma' = \mu_2' \tan\alpha \qquad \text{(B-7)}$$

which is identical in form to Eq. (15a), but σ', μ_2', a are now defined as in Eqs. (B-5), (B-6); the anti-symmetric case leads again to Eq. (15b) in form but with the modified parameters above.

Analytically, then, the heated jet case appears little different from the unheated case. The magnitude of $|\bar{s}|^2$ is decreased by the numerator factor $(T_a/T_1)^2$. The location of the spikes (in θ) and the range of values of K_1 where spikes may be expected has changed (i.e. Fig. 14b must be modified to accomodate the new definition of a and $K^2 > (c_a/c_1)^2$), but otherwise the problem is qualitatively similar to the unheated case.

When one considers an actual numerical example, however, the shift in the K_1-range where spikes are possible can be of major significance. The occurrence of spikes for this configuration requires, as pointed out earlier in the report, that a be real (corresponding to a wave-type solution in the central high-velocity part of the jet) when $|K_1|$ is large* (exponential-type solutions in the outer layer of the jet). Heating the jet can have the effect of shifting the K_1-range where a is real away from the very high values of $|K_1|$. Fewer spikes may then be encountered, or possibly only pressure peaks of moderate magnitude.

An example may serve to clarify these points. Consider a jet with

$$M_0 = 2.9 \qquad\qquad a_1/a_2 = 0.6777$$
$$M_1 = 1.5 \qquad\qquad S_T = 0.2$$

For the _unheated_ jet $(T_0=T_1=T_a)$ a is real for $180^\circ > \theta > 121.76^\circ$ (and also for $104.86^\circ > \theta > 0$, but this part of the θ-range produces no spikes and so is not of interest here). Within the range of interest a increases with increasing θ from $a = 0$ at $\theta = 121.76^\circ$ to $a = \infty$ at $\theta = 131.81^\circ$ (the Mach angle corresponding to $M_1 = 1.5$); a then decreases with further θ increase to $a = 228.61^\circ$ at $\theta = 180^\circ$. Within this a-variation, an infinite number of solutions of Eq. (B-7) is possible.

---

* As before, numerical solutions are considered only for the plane $y = 0$, where $K_2 = 0$ and $K = |K_1|$.

However, if the jet is heated so that $T_0 = 3T_a$, $T_1 = 2T_a$, the velocities remaining as above, it is found that α is real for $180° > \theta > 148.89°$ (and for $102.47° > \theta > 0$, which is less of interest). In this range $2 < K_1 < 3.01$ *. That is, K_1 takes on only moderate values, and only moderate pressure peaks are encountered. Also, α increases with increasing θ from $\alpha = 0$ at $\theta = 148.89°$ to $\alpha = 63.60°$ at $\theta = 180°$. With this limited range of α-variation permitted, not more than one solution (if any) of Eq. (B-7) is probable.

Thus a velocity distribution which resulted in an infinite number of spikes in the far-field pressure distribution for the source in the <u>un-heated</u> jet has at most one somewhat moderate pressure peak when the jet is heated with the temperature ratios indicated. This change is probably related to the fact that the actual (local) Mach number of the jet, based on local temperature, is greatly reduced. (Of course, one can find examples where the Mach number and temperature ratios are such that multiple spikes will occur for the heated jet also.)

----

* Recall that $K_1 = \cos\theta / (1 + M_1 \cos\theta)$.

References

1. Graham, E. W. and Graham, B. B.: Theoretical Study of the Effects of Refraction on the Noise Produced by Turbulence in Jets. NASA CR-2390, 1974.

2. Maestrello, L.: On the Relationship Between Acoustic Energy Density Flux Near the Jet and Far-Field Acoustic Intensity. NASA TN D-7269, 1973.

3. Gottlieb, P.: Acoustics in Moving Media. PhD Thesis, Department of Physics, M.I.T., 1959.
   Gottlieb, P.: Sound Source Near a Velocity Discontinuity. J. Acoust. Soc. Am., 32, 1960, pp. 1117-1122.

4. Moretti, G. and Slutsky, S.: The noise field of a subsonic jet. Gen. Appl. Sci. Labs. GASL Tech. Rep. 150 (AFOSR TN-59-1310), 1959.

5. Mani, R.: A Moving Source Problem Relevant to Jet Noise. J. Sound & Vibr. 25 (2), 1972, pp. 337-347.

6. Schubert, L.K.: Numerical Study of Sound Refraction by a Jet Flow. II. Wave Acoustics. J. Acoust. Soc. Am., 51, 1972, pp. 447-463.

7. Liu, C. H. and Maestrello, L.: Propagation of Sound Through a Real Jet Flowfield. AIAA Paper 74-5, 1974.

8. Padula, S. L. and Liu, C.H.: A Computing Method for Sound Propagation Through a Nonuniform Jet Stream. Paper presented at the 88th Meeting of the Acoustical Society of America, 1974.

9. Morfey, C. L. and Tanna, H. K.: Sound Radiation from a Point Force in Circular Motion. J. Sound & Vibr. 15, 1971, pp. 325-351.

10. Ingard, U. and Singhal, V. J.: Upstream and Downstream Sound Radiation into a Moving Fluid. J. Acoust. Soc. Am. 54, 1973, pp. 1343-1346.

11. Graham, E. W. and Graham, B. B.: Effect of a Shear Layer on Plane Waves of Sound in a Fluid. J. Acoust. Soc. Am. 46, 1969, pp. 169-175.

12. Graham, E. W. and Graham, B. B.: The Acoustical Source in a Two-Dimensional Jet. Boeing Sci. Res. Labs. Doc. D1-82-0909, 1969.

13. Graham, E. W.: A Sequence of Transient Acoustical Sources in an Idealized Jet. Boeing Sci. Res. Labs. Doc. D1-82-1002, 1970.

14. Graham, E. W. and Graham, B. B.: Transient Acoustical Sources in an Idealized Jet. J. Acoust. Soc. Am. 52, 1972, pp. 221-226.

15. Graham, E. W. and Graham, B. B.: A Note on Theoretical Acoustical Sources in Motion. J. Fluid Mech. 49, 1971, pp. 481-488.

16. Graham, E. W. and Graham, B. B.: Review of Some Acoustical Source Problems and Far Field Integration Methods. Boeing Sci. Res. Labs. Doc. D1-82-0788, 1968.

17. Gradshteyn, I. S. and Ryzhik, I. M.: Table of Integrals, Series, and Products. Academic Press, New York and London, 1965.